Final thesis

Auteur : Buckinx, Emma
Promoteur(s) : Mahieu, Emmanuel; Grodent, Denis
Faculté : Faculté des Sciences
Diplôme : Master de spécialisation en cosmos exploration
Année académique : 2020-2021
URI/URL : http://hdl.handle.net/2268.2/11942

University of Liège

Faculty of Sciences

Department of Astrophysics, Geophysics and Oceanography

Infrared Group of Atmospheric and Solar Physics

Is the covid-19 lockdown affecting air quality above the Jungfraujoch Observatory?

MASTER'S THESIS

Emma BUCKINX

Promotor: Dr. Emmanuel Mahieu

Co-promotor: Prof. Dr. Denis Grodent

Master's Thesis submitted for the degree of Master in Cosmos Exploration

Academic year 2020/2021

Acknowledgements

Hereby I put the finishing touches to the writing of my master's thesis to obtain my master's degree in Cosmos Exploration at the University of Liège. This road was interesting, fascinating, challenging, but most of all worthwhile. I am very grateful to have spent the final months of my study career at the Infrared Group of Atmospheric and Solar Physics. Although this was unfortunately only remotely, I have been given many opportunities to learn, to experience and to grow personally as well as a scientist. Thank you all!

Especially, I would like to thank Dr. Emmanuel Mahieu, my promotor and head of GIRPAS for his excellent guidance during this few months. You were a great help throughout the whole process of writing this thesis both as a mentor and specialist in the field. A special thank you is given for your time and effort to learn a complete newcomer like me the basics of a whole new research field, especially during these strange times of the pandemic. Despite my medical background, you have triggered my interest in science of the Earth and helped me to further develop it. Although we have never had the chance meet in person, you were an enormous support.

I also want to thank Prof. Dr. Denis Grodent for his help as my co-promotor. Your advises and expertise have guided me throughout the writing of this master's thesis. Thank you for your great insights and opinions to further improve this work. I appreciate your support and trust.

I can definitely not forget to thank the organisers of this specialised master program to be given the chance to explore this whole new science field. I believe this one-year studies is a major contribution to my master's degree in biomedical sciences, and I am convinced now that I want to explore this field even more. The pandemics have not made it easy to both of us, however, you made me feel supported and appreciated during this whole journey.

I am also very thankful to Dr. Bruno Franco, Dr. Michaël De Becker and my supervisors for reading and evaluating this master's thesis.

A final thanks goes to my parents, sister and friends who always supported me during this period and indirectly played an important role in this accomplishment.

Abstract

In mid-March 2020, a global lockdown was enforced in order to minimise the spread of the covid-19 virus. This lockdown has had an enormous impact on the entire world as human activity was significantly reduced. In relation to this, multiple studies have shown that some well-known air pollutants had global decreased emissions and abundances in the atmosphere during this specific period of time. The aim of this master's thesis is to study the abundances of multiple tropospheric air pollutants, monitored at the Jungfraujoch Observatory (Switzerland), in the context of the covid-19 lockdown.

The main goal of this work is to compare the 2020 abundances of a suite of air pollutants routinely monitored at the Jungfraujoch to their mean levels derived from the last 10 or 20 years. In a first part of this work, reference multiyear time series of the selected air pollutants were constructed and then used for comparison with their abundances measured in the year 2020. Mixing ratios and total columns retrieved from Fourier-Transform infrared spectra recorded at Jungfraujoch were used for this purpose.

The concentrations of the individual air pollutants showed that in the first half of year 2020, the abundance of multiple species was reduced in comparison to the multiyear time series. More specifically, C_2H_2, C_2H_4, C_2H_6, CH_3OH, H_2CO, HCOOH and tropospheric O_3 concentrations were reduced during lockdown. However, for CH_4, CO, HCN and NH_3, no concluding or robust evidences of an effect of lockdown on their abundances was found. This strongly suggests that the observed drop in tropospheric O_3 concentrations during the first half of the year 2020 was more related to a decrease in VOCs rather than being influenced by the other important precursors, namely CH_4 and CO. Further analysis of these results should be performed in order to quantify these variations in abundances. Also, additional studies, including model data, will be needed to find a potential correlation between the covid-19 lockdown and reduced abundances for some species, and to evaluate the reductions in their emissions.

From these results, we can conclude that most of the studied tropospheric air pollutants above the Jungfraujoch Observatory experienced a reduction of their abundances, contributing to lower air pollution during the 2020 lockdown for a remote sit. Further research is needed to clarify and quantify to what extent the covid-19 lockdown has contributed to this atmospheric change

Contents

Acknowledgements i

Abstract ii

Contents iii

List of abbreviations v

Introduction 1

1. Air pollutants in the Earth's troposphere 4

1.1. The troposphere 4

1.1.1. The troposphere as a part of the Earth's atmosphere 4

1.1.2. Structure of the troposphere 6

1.1.3. Temperature 7

1.1.4. Pressure and density 8

1.1.5. Composition 8

1.1.6. Tropospheric air transport 10

1.1.7. Oxidizing capacity of the troposphere 13

1.2. Air pollution in the troposphere 14

1.2.1. Definition 14

1.2.2. Primary air pollutants 15

1.2.3. Secondary air pollutants 17

1.3. Included tropospheric air pollutants 20

2. Data retrieval at the Jungfraujoch Observatory 22

2.1. The International Scientific Station of the Jungfraujoch 22

2.2. Data retrieved from infrared spectra 24

2.2.1. The principle behind infrared spectroscopy 24

2.2.2. Fourier-Transform InfraRed Spectrometer: spectra generation 25

2.2.3. Analysis of the spectra 27

3. Construction of reference multiyear time series 29

3.1. Raw data processing 29

3.1.1. Data selection and filtering 29

3.1.2. Calculation of monthly means 30

3.2. Trend analysis 30

3.2.1. Bootstrap resampling trend analysis 31

3.2.2. Statistical analysis 32

3.3. Detrending the data 33
3.4. Correction of the data 34
3.5. Interpretation 36
3.5.1. Interpretation of the trends 36
3.5.2. Interpretation of the seasonal cycles 37
4. Evaluation of the effect of lockdown on the abundance of the included air pollutants....39
4.1. Defining the lockdown period 39
4.2. Comparison between the reference multiyear time series and 2020 monthly means of the individual air pollutants 41
4.2.1. Data processing 41
4.2.2. Acetylene 41
4.2.3. Ethylene 42
4.2.4. Ethane 44
4.2.5. Methane 45
4.2.6. Methanol 46
4.2.7. Formaldehyde 47
4.2.8. Hydrogen cyanide 48
4.2.9. Formic acid 48
4.2.10. Carbon monoxide 49
4.2.11. Ammonia 50
4.2.12. Tropospheric ozone 51
4.3. The average change in tropospheric ozone precursors during lockdown 53
4.3.1. The VOCs 53
4.3.2. Carbon monoxide and methane 55
4.4. Future research perspectives 55
5. Conclusions 57
6. References 59

List of abbreviations

ABL	Atmospheric Boundary Layer
BC	Black Carbon
DOFS	Degrees Of Freedom for Signal
EEA	European Environment Agency
EJC	Engineers Joint Council
FITRMS	Fitted Root Mean Square
FTIR	Fourier Transform InfraRed
FTS	Fourier Transform Spectrometer
GHG	Greenhouse Gas
GIRPAS	Groupe Infrarouge de l'Atmosphère Physique et Solaire
ISA	International Standard Atmosphere
ISO	International Organization for Standardization
IR	InfraRed
ISSJ	International Scientific Station of the Jungfraujoch
NCAR	National Center for Atmospheric Research
NCEP	National Centers for Environmental Prediction
NDACC	Network for Detection of Atmospheric Composition Change
NMVOC	Non-Methane Volatile Organic Compound
NOAA	National Oceanic and Atmospheric Administration
NPL	National Physical Laboratory
PBL	Planetary Boundary Layer
PM	Particulate Matter
ppv	particles per volume
SD	Standard Deviation
UV	Ultraviolet
VOC	Volatile Organic Compound
WHO	World Health Organisation

Introduction

"Be safe, be smart, be kind" - *Dr. Tedros Adhanom Ghebreyesus, WHO Director General (March 2020)*

These words can nowadays be immediately linked to their context. Covid-19. The most far-reaching global impact known to mankind in the past century. At the time of writing, many countries are still fighting the covid-19 virus. Hence the importance of Dr. Tedros' words, safety, smartness and kindness get us through these difficult times where the world is ruled by a pandemic.

By mentioning that the world is ruled by a pandemic, it means the world in its entirety. Apart from the human population of the Earth, other aspect related to our planet seem to be affected in a more indirect way. Global lockdowns have a drastic impact on local and global economies, changes in energy demand patterns are observed and even animals and plants notice this severe human health threat. Although many other consequences still need to be studied and discussed, it is already safe to say that a worldwide pandemic slows down most human activities.

This leads us to the main subject of this master's thesis. While mankind slowed down its activities, did this affect our impact on climate change? We cannot hide the fact that the Earth is warming up. According to the National Centers for Environmental Information of the National Oceanic and Atmospheric Administration (NOAA), an uninterrupted increase of yearly temperature anomaly is observed since 1977. In 2020 and 2016, the highest differences were seen with a temperature anomaly of 1.17°C and 1.23°C, respectively (NOAA National Centers for Environmental information, 2021). This global warming, as it is called, introduces significant changes in the Earth's climate. Although climate change is not specifically a thing of today, we must admit that since the mid-20s there is a large human impact on the Earth's climate system. We are increasingly moving faster towards a more technologically advanced civilization. This privilege can be used in a positive manner, however, unwittingly we also affect our planet on a much larger scale.

But what if we actually find ourselves in a situation that forces us to stop, or just slow down? During the covid-19 pandemic, we had to retreat ourselves into our homes. A global lockdown in March 2020 resulted in empty streets, carless roads, many factories at a standstill missing their black plumes of smoke, a sky that was again ruled by birds and not by planes. Interestingly, this list of human activities that are put on hold can be related to the emission of a significant part of gases affecting the air quality and so climate change. Indeed, gases like for example carbon monoxide, methane, ammonia and several volatile organic compounds

are well known air pollutants partially resulting from human activity. As many of these air pollutants affect the amount of incoming sunlight by reflection or absorption, they have a significant contribution to global warming and so climate change. Important to note is that most of them are not direct greenhouse gases (GHGs). A GHG is defined as a gas present in the Earth's atmosphere that has the property to absorb infrared radiation emitted from the ground and reradiating a significant part back to the Earth. The air pollutants have a primary impact on air degradation, and as such they influence the oxidative capacity of the troposphere (see section 1.1.7). In case of a decreased oxidative capacity, a major primary GHG like methane (CH_4) will lose an important sink and have a more pronounced effect on global warming as its lifetime will increase.

In the context of the covid-19 pandemic, a recent study of Bauwens et al. observed an average nitrogen dioxide (NO_2) column drop in the first months of 2020 over all Chinese cities, Europe and the United States of about 20% to 40% in comparison with 2019 (Bauwens et al., 2020). NO_2 is an air pollutant that is dominant in the upper troposphere and plays a key role in the formation of tropospheric ozone and the hydroxyl radical (OH) (see section 1.2.3.). Another study of Steinbrecht et al. has also shown that the year 2020 was a period of reduced tropospheric ozone across the Northern Hemisphere (Steinbrecht et al., 2021). Tropospheric ozone is a major air pollutant that is produced out of different series of reactions between sunlight and pollutants directly emitted from the Earth's surface. These mainly include volatile organic compounds and nitrogen oxides but also other gases like methane and carbon monoxide. To take this observation a step further, it might be interesting to study the abundances of some air pollutants related to ozone production and human activity in the context of the covid-19 pandemic.

Several of the indicators of air quality, and so air pollution, are available among the targets of the Jungfraujoch Fourier Transform InfraRed (FTIR) monitoring program. Therefore, the main goal of this master thesis is to compare the abundance of multiple air pollutants in 2020, retrieved at the International Scientific Station of the Jungfraujoch (ISSJ), to climatological data based on the measurements available for the last one or two decades. The ISSJ is located in the Swiss Alps (46.55°N, 7.98°E, 3580 m above sea level). The "Groupe InfraRouge de Physique Atmosphérique et Solaire" (GIRPAS, Institute of Astrophysics and Geophysics, University of Liège) monitors solar radiation in the infrared at this station.

The following pages of this master thesis manuscript will provide an in dept description on the background of this topic. More specifically, the troposphere and its characteristics will be discussed, together with an overview of the main tropospheric air pollutants and the ones included in this study. In a second part, data retrieval followed by data processing of the

selected species will be explained. Results of this processing will be presented together with the analysis of the different time series and their comparison with the year 2020. All findings will be accompanied by a discussion and interpretation. Finally, the manuscript will end with an overall conclusion and some perspectives for the future.

In order to have a proper answer to the question whether the covid-19 pandemic has influenced or is still influencing the Earth's climate, a lot of research will be needed. This master thesis study will therefore be a very small but significant step in developing an answer to a question of great importance.

1. Air pollutants in the Earth's troposphere

1.1. The troposphere

The troposphere is the lowest layer of Earth's atmosphere extending from the ground to an average altitude of about 13 km. This layer is of great importance since it contains the air that we breath. The troposphere can be further divided in the free troposphere (upper layer) and the atmospheric boundary layer (lower layer), with nearly all weather conditions taking place in the latter one (see section 1.1.2.). In this first part of the master thesis manuscript, the troposphere and its characteristics will be described in more detail.

1.1.1. The troposphere as a part of the Earth's atmosphere

The atmosphere of the Earth is the collection of gases or layers of gases surrounding our planet, trapped by the Earth's gravitational field. By volume, its main composition is defined by nitrogen (±78%), oxygen (±21%), argon (±0.9%) and carbon dioxide (±0.04%). Our atmosphere provides an important protection for life because of its ability to absorb ultraviolet (UV) radiation as well as higher energy radiations (x-rays) coming from the sun. In addition, it can heat the Earth's surface providing favourable temperatures for life as we know it and it damps out diurnal variations in temperature on the ground.

The general atmospheric stratification describes different layers as a reversal of the temperature gradient, or in other words, the variation of temperature with altitude. With the troposphere being the first layer, the next ones from bottom to top are the stratosphere, the mesosphere, the thermosphere and the exosphere. An overview of all these different layers is given in Figure 1.1. The variation in temperature gradient can be attributed to the presence of different gases at different altitudes, each of them interacting in a particular way with the incoming sunlight. For example, in the stratosphere the temperature increases with altitude. This is due to the fact that 90% of the total ozone is distributed in the stratosphere. This stratospheric ozone, better known as the ozone layer, absorbs almost 98% of the solar radiation with wavelengths between 200 nm and 300 nm, thereby strongly heating up the air at this altitude. The same accounts for the increasing temperature in the thermosphere, considering absorption of solar radiation of about 200 nm wavelength, mainly by O_2. In the mesosphere, the coldest atmospheric temperatures of about -143°C are reached. These low temperatures can be attributed to the presence of carbon dioxide and nitrogen monoxide emitting infrared radiation and thereby cooling down the atmosphere. This also explains the

negative temperature gradient of the mesosphere as shown in Figure 1.1. The temperature decrease in the troposphere mainly results from the expansion of the gas with altitude. On average, the temperature gradient in the troposphere is -6.5°C per 1,000 m of altitude (International Organisation for Standardisation, 1975).

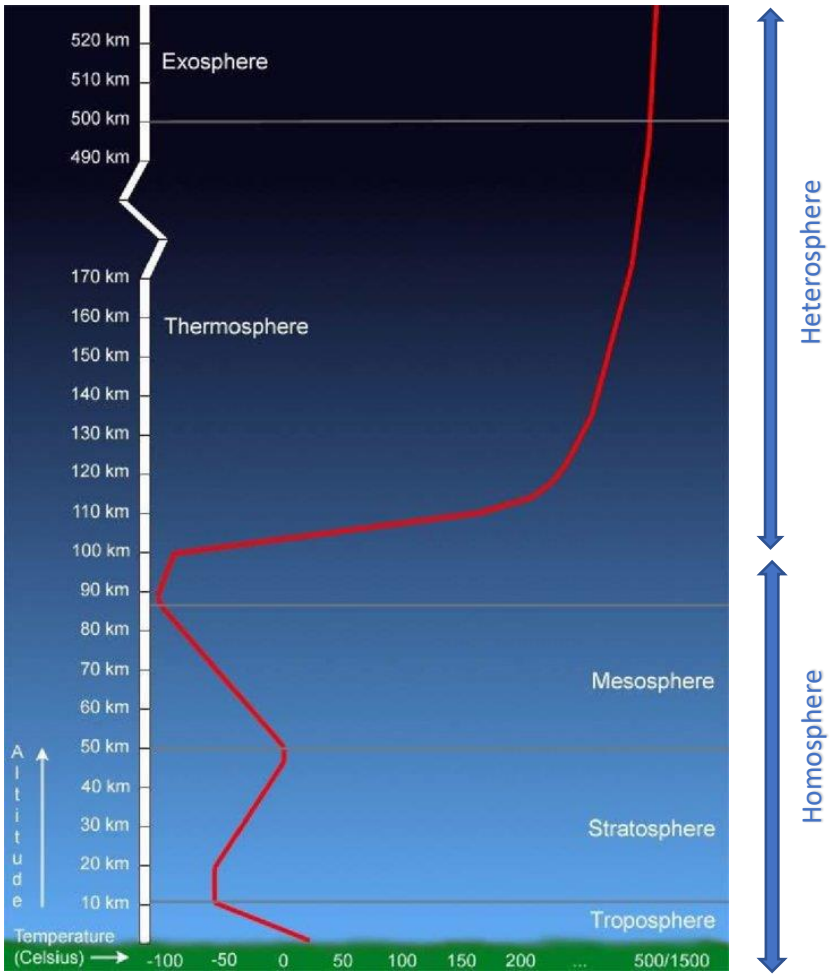

Figure 1.1. The average temperature profile of Earth's atmosphere

Each atmospheric layer has a boundary related to the region where the temperature gradient inverses. This inversion layer is also called a "pause", giving us the mesopause (at about 85 km), the stratopause (at about 50 km) and the tropopause with a mean altitude varying between 18 km at the equator and 8 km at the poles. Near the mesopause, another boundary can be defined, namely the turbopause, also known as the homopause. The turbopause, at an altitude of about 100 km, divides the Earth's atmosphere into the homosphere, which is the lowest layer, and the heterosphere or upper layer (see Figure 1.1). Below the turbopause, inert constituents are well mixed. In the heterosphere, this is not the case because of molecular diffusion. Here, an exponential decrease of partial pressure of one constituent as a function of

its own scale height is observed. For example, light constituents like hydrogen or helium have a large scale height. This means that their partial pressure slowly decreases with altitude and so these become more abundant at higher altitudes in comparison with heavier constituents.

1.1.2. Structure of the troposphere

Two specific regions can be distinguished in the troposphere: the atmospheric boundary layer (ABL), starting from the ground up to an average altitude of 1 km, and the free troposphere above ending up at the tropopause. This is schematically represented in Figure 1.2.

The ABL can be defined as the region of the atmosphere that is directly in contact with the continental or oceanic surface. This is the place where most human activities and emissions occur. With a typical thickness of 1 km, ranging from about 100 m to a few kilometres in the mid-latitudes, the ABL contains about 10% of the total atmospheric mass. This region strongly responds to changes in solar radiation that reaches the ground causing diurnal cycles of the continental land surface temperature. High turbulence rates in this region make this a privileged zone for energy exchange and mixing of air masses. This turbulence is due to the drag of the Earth's surface on the wind and buoyancy forces related to the warmer lower layers (Smith, 1975).

The free troposphere (Figure 1.2. Free Atmosphere), on the other hand, is the location of important weather and climate processes. It holds greenhouse gases, clouds and water vapour and provides horizontal and vertical transport of energy and mass. It is also characterised by a constant mixing ratio of sufficiently long-lived gases.

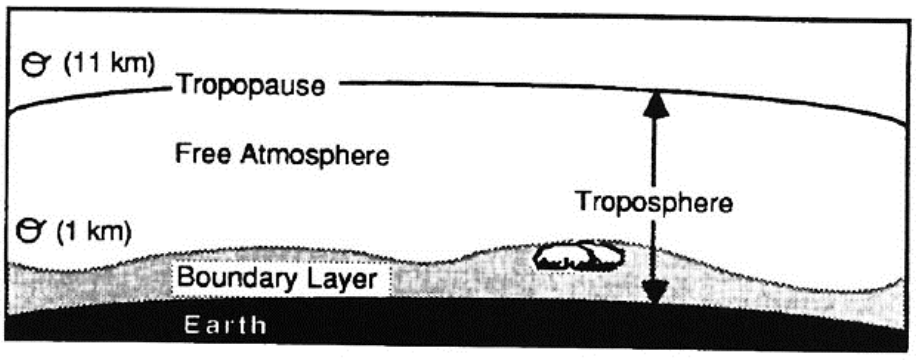

Figure 1.2. Troposphere division: boundary layer and free atmosphere. (Stull, 1988)

1.1.3. Temperature

As mentioned before, the troposphere is characterized by a negative temperature gradient. Starting from sea level, the temperature drops from an average of about 15°C to about -51°C at the tropopause. According to the International Standard Atmosphere (ISA)[1], the temperature decreases with altitude at a constant rate of -6.5°C/1000m up to the tropopause, with a standard tropopause altitude of 11,000 m.

Most of the solar energy is absorbed by the ground. Rock, soil and water absorb this radiation, mainly in the visible spectrum, and radiate it back as infrared radiation or heat. The air of the lowest levels of the atmosphere warms up through convection and rises up. Due to buoyancy forces and the adiabatic property of air (i.e. few energy transport by heat) the rising hot air is allowed to cool down and move back in the direction of the ground. This vertical transport process of air (convection) only takes place at the troposphere and explains the turbulent mixing of air in the lowest part of the atmosphere. Clouds present in the troposphere contain important gases, such as methane, ammonia, sulphuric acid and water vapour, absorbing the IR radiation emitted from the surface and thereby allowing more stable temperatures on Earth throughout the day and night. These different processes of heat transfer in the atmosphere are illustrated in Figure 1.3.

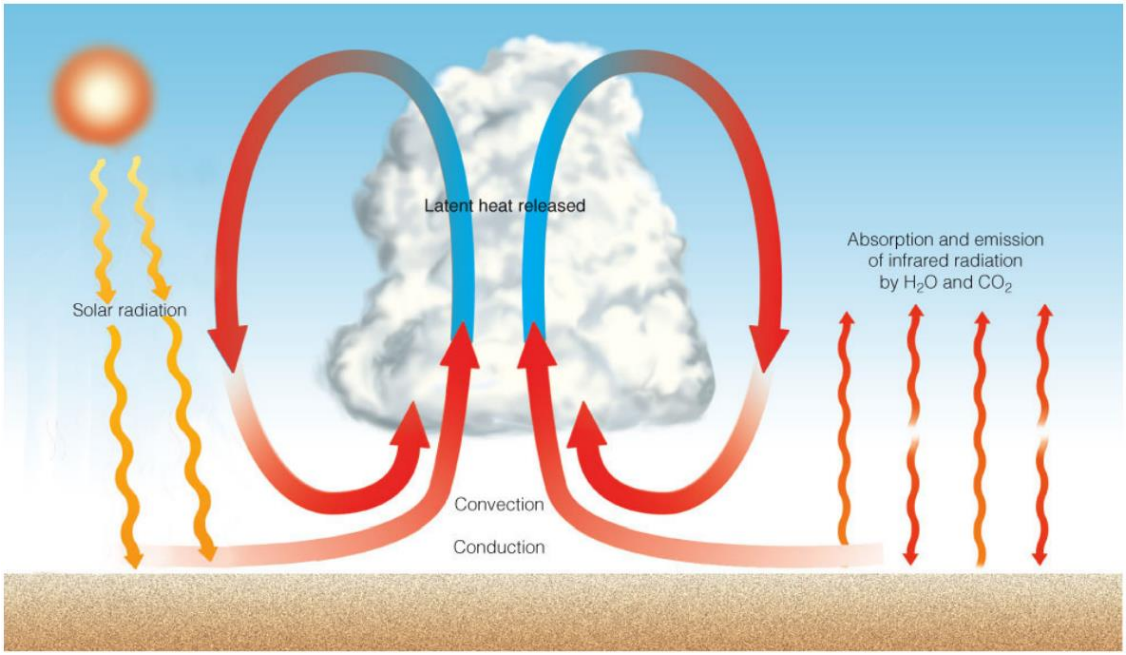

Figure 1.3. The different ways of heat transfer in the Earth's atmosphere. (Thomson Higher Education)

[1] The International Standard Atmosphere is a static atmospheric model describing how pressure, temperature, density, and viscosity are changing over a wide range of altitudes or elevations, published by the International Organization for Standardization (ISO) as an international standard (ISO 2533:1975). (International Organisation for Standardisation, 1975)

1.1.4. Pressure and density

The pressure of air reaches a maximum at sea level and decreases with altitude. In the troposphere, it ranges from 1000 to 200 millibars (Figure 1.4.). Also, the atmospheric density generally decreases with altitude. The troposphere is typified by a relative dense air because it contains more than 75% of the mass of the entire atmosphere. According to the ISA, the standard density of dry air (as an ideal gas) at sea level is 1.225 kg/m^3. (International Organisation for Standardisation, 1975)

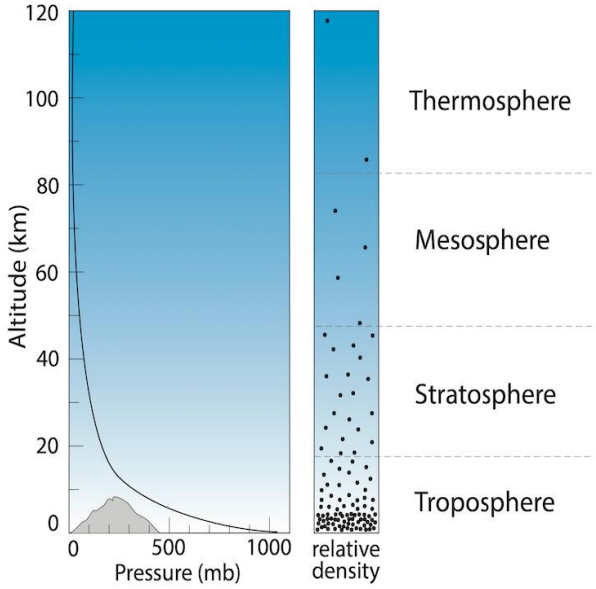

Figure 1.4. Pressure and density profile of Earth's atmosphere.

1.1.5. Composition

The Earth's atmosphere is mainly comprised of nitrogen (N_2), argon (Ar) and oxygen (O_2), which are also referred to as the major constituents. They have a volume ratio (vol%) of 78.08 vol%, 20.95 vol% and 0.93vol%, respectively and make up more than 99% in volume of our atmosphere (D.C.Catling, 2015). Minor constituents are carbon dioxide (CO_2), stratospheric ozone (O_3), methane (CH_4), nitrous oxide (N_2O), sulphur dioxide (SO_2) and water vapour (H_2O), with other gases present in trace amounts. The major atmospheric components show a rather constant concentration over time and location, whereas the minor ones seem to vary significantly. Although only making up less than 1 percent of the atmosphere, the variable minor atmospheric components have a large influence on both short-term weather and long-term climate.

Gases playing an important role in the chemical composition of the troposphere are thus present in very small amounts and are listed in Table 1.1. Water vapour and carbon dioxide are the most important tropospheric gases.

H_2O	water vapour	0.01 – 0.4 vol%
CO_2	carbon dioxide	360 ppm
CH_4	methane	1.7 ppm
N_2O	nitrous oxide	310 ppb
CO	carbon monoxide	50-500 ppb
O_3	ozone	10-80 ppb
SO_4	sulphate	20 ppt - 2 ppb
NO_2	nitrogen dioxide	1 ppt- 10 ppb
OH	hydroxyl radical	0.01-0.1 ppt

Table 1.1. Important tropospheric gases expressed as volume mixing ratios. ppm, particle per million; ppb, particle per billion; ppt, particle per 1000 billion. [from the website of the Royal Belgian Institute for Space Aeronomy]

Water vapour is mostly concentrated near the surface of the Earth. There is a permanent H_2O exchange and transport between all reservoirs on Earth via mainly evaporation and condensation leading to cloud formation and rainfall. This is also called the hydrological cycle. With a relative low residence time in the atmosphere of about 9 days, water vapour shows therefore relative strong variations with season and latitude. Water is essential to the development and preservation of life on Earth and is moreover the main greenhouse gas in our atmosphere with a contribution of about 55% to the Earth's greenhouse effect. Water is mainly of importance in the troposphere because of its role in the oxidation of several atmospheric compounds, such as for example methane (Inglezakis et al., 2016).

Carbon dioxide has a volume mixing ratio of about 360 particles per million (ppm) and belongs to the most important tropospheric gases. Moreover, it is a major greenhouse gas of anthropogenic source with a relative long lifetime of a few centuries (Royal Belgian Institute for Space Aeronomy, 2021).

A more detailed discussion on some of these components will follow in the section about air pollutants (section 1.2.).

1.1.6. Tropospheric air transport

Vertical and horizontal distribution of trace gases in the troposphere are driven by global atmospheric circulation which acts as a response to differences in temperatures at the equator (warm) and the poles (cold). Knowledge of this global circulation is of great importance to understand the distribution of the gases with a relatively long lifetime in the atmosphere and in this case, the troposphere.

a. Global atmospheric circulation

As seen in section 1.1.3. convection cells redistribute heat when hot air rises, cools down and eventually moves back to the surface of the Earth. There are three types of major convection cells in the troposphere, namely the Hadley cells, the polar cells and the Ferrel cells, which exist in both the northern and southern hemispheres. These cells are illustrated in Figure 1.5. At the equator, temperatures are higher because of the more intense incoming solar radiation. This warm and wet air rises up creating a low pressure and cools down at higher altitudes stimulating cloud formation via the process of condensation. The cold air now moves in both northern and southern directions and eventually sinks at around 30° north and south of the equator. This typical convection cell is called the Hardley cell. For the polar and Ferrel cell, warm air rises at around 60° north and south of the equator and sinks at 90° and 30° respectively. This circulation of air is also called the meridional circulation as the air travels along a meridian.

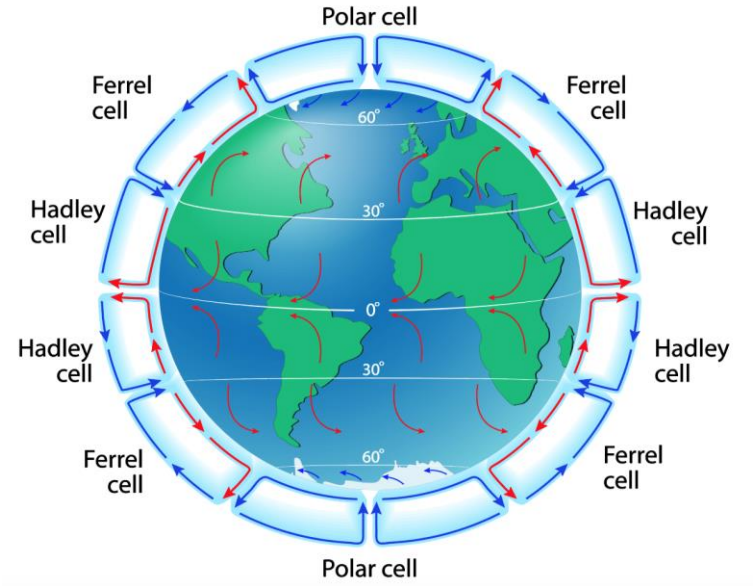

Figure 1.5. Global atmospheric circulation model.

The specific heat transfer mechanism of each cell has an important influence on the weather patterns in the troposphere and on zonal air circulation. Low pressure regions (where the air rises up), typically show high rainfalls, whereas high pressure regions (where the air sinks) are dry areas.

Considering the zonal circulation, or air circulation along a latitude circle, it is known that the air moving towards the equator on the lower part of the Hadley cells is deflected by the Coriolis force. This Coriolis force is a fictious force resulting from the fact that the Earth is spinning and therefore is a rotating frame of reference. The Coriolis force depends on latitude, it maximizes at the poles and is zero at the equator. Figure 1.5. illustrates this situation near the equinoxes. Between 30° north and south of the equator, air is deflected towards the west for both hemispheres. The surface wind in the Ferrel cells moves towards the poles and is also deflected to the right in the northern hemisphere and to the left in the southern hemisphere by the Coriolis force. The same principle accounts for the surface air of the polar cells.

b. Vertical transport

Pollutants emitted from the surface can cause harmful effects to human health and vegetation when staying at the boundary layer. However, they can also be transported to the free troposphere and influence the Earth's climate. Trace gases need to have lifetimes long enough in order to reach higher layers of the atmosphere.

Beside convection, advection[2] and turbulent mixing of air also contribute to the vertical transport of air in the troposphere (Donnell et al., 2001).

Figure 1.6. illustrates the different time scales for trace gases to vertically migrate in the atmosphere. Within 1 – 2 days air pollutants emitted from the surface have the ability to reach the top of the ABL (figure 1.6.: PBL = planetary boundary layer; refers to ABL). In one week, air can reach the beginning of the troposphere and end up at the tropopause around one month of traveling from the surface. In order to reach a certain altitude in the stratosphere, much longer lifetimes of the trace gases are needed. Because of the lack of turbulent mixing in this region, it can take 5 – 10 years (Brasseur & Jacob, 2017).

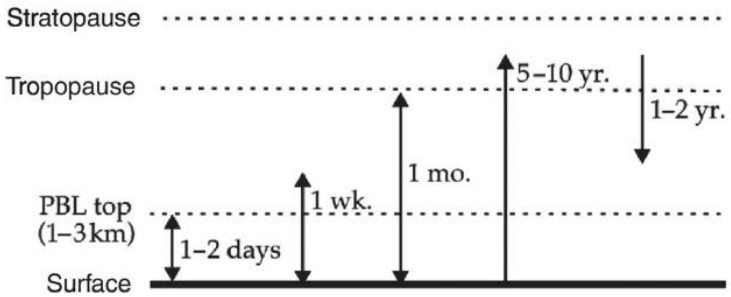

Figure 1.6. Time scales for vertical atmospheric transport of trace gases (Brasseur & Jacob, 2017)

c. Horizontal transport

As shown in Figure 1.7. horizontal transport on Earth is fastest in the longitudinal direction with wind speeds of the order of 10 m/s. It would only take a few weeks for air to travel around the whole globe. Meridional transport takes much longer. Wind speeds are of the order of 1 m/s so air needs about 1 – 2 months to travel from the equator to the polar regions. Interhemispheric exchange takes even longer. About one year is needed for air to exchange between the northern and southern hemispheres (Brasseur & Jacob, 2017)

[2] The process of transport of an atmospheric property solely by the mass motion.

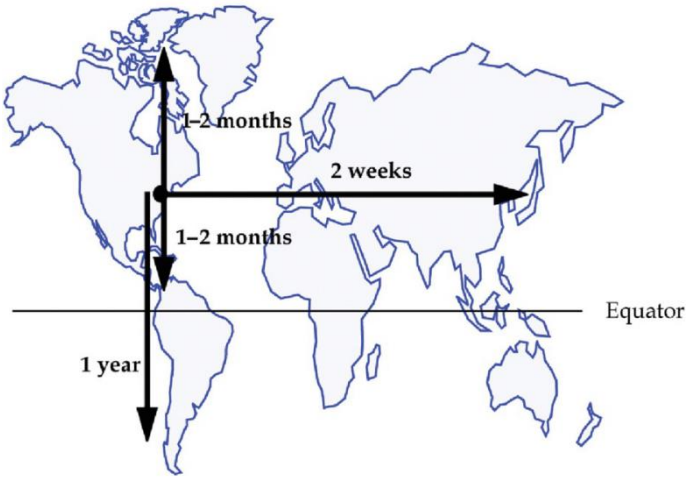

Figure 1.7. Time scales for horizontal atmospheric transport of trace gases (Brasseur & Jacob, 2017)

1.1.7. Oxidizing capacity of the troposphere

The atmospheric boundary layer together with the free troposphere typically are oxidizing environments. In other words, these regions of the atmosphere have the capacity to oxidize important tropospheric compounds thereby critically influencing the lifetime of directly emitted gases at the surface. On the other hand, this oxidation can, as a consequence, favour the formation of other gases in the atmosphere. The oxidizing capacity of the troposphere is therefore an important feature as it destructs and produces many gases.

A major oxidant in the troposphere is the hydroxyl radical (OH). It reacts more slowly with O_2 compared to other compounds and thus reaches lifetimes that are relatively long for a radical (ranging from 1 second to 1 minute). Other important atmospheric oxidizing compounds of the troposphere are other radicals in the HO_x family such as hydroperoxyl (HO_2) and peroxyl (RO_2)[3]. These radicals are formed in the troposphere in reactions that start with photolysis of ozone originating from the stratosphere. To give an example, OH is formed as follows[4]:

$$O_3 + h\nu \rightarrow O_2 + O(^1D) \quad (1)$$

$$O(^1D) + H_2O \rightarrow 2OH \quad (2)$$

[3] R is a radical or alkyl saturated carbon chain
[4] $O(^1D)$ is the first excited state of atomic oxygen

OH formation is initiated by tropospheric ozone, UV radiation and water vapour. This means that regions with the highest humidity (the tropics) have the highest OH levels (Lelieveld et al., 2002).

More details on how OH can be used to form ozone will be given in the section on secondary air pollutants (section 1.2.3).

1.2. Air pollution in the troposphere

Air pollution is a general term used for substances present in the atmosphere that cause any harm to the planet in its entirety. This includes the planet itself but also living beings, materials and the Earth's climate. Amongst the different type of air pollutants, homogeneous (gases) and heterogeneous (aerosols) pollutants can be distinguished. In this study, we focussed on a selection of gaseous tropospheric air pollutants. A brief explanation on the major air pollutants will be given in the next sections, followed by an overview of the ones that were included in this study.

1.2.1. Definition

Air pollution is defined by the Engineers Joint Council (EJC) and the World Health Organisation (WHO) as "the presence in the outdoor atmosphere of one or more contaminants, such as dust, fumes, gas, mist, odour, smoke, or vapor, in quantities, of characteristics, and of duration such as to be injurious to human, plant or animal life or to property, or which unreasonably interferes with the comfortable enjoyment of life and property" (World Health Organization, 1980). Air pollutants can be of biogenic (natural) and/or anthropogenic (human-made) nature and have multiple types of sinks. There are two main types of air pollutants: the primary and secondary air pollutants. Primary air pollutants are directly emitted compounds having variable lifetimes that are mostly detected close to the place of emission. Secondary pollutants result from chemical transformations having a rather short lifetime and cause pollution on a larger scale. These often have stable reservoirs that can be activated under certain well-defined conditions. Figure 1.8. provides an overview of the main air pollutants present in the atmosphere.

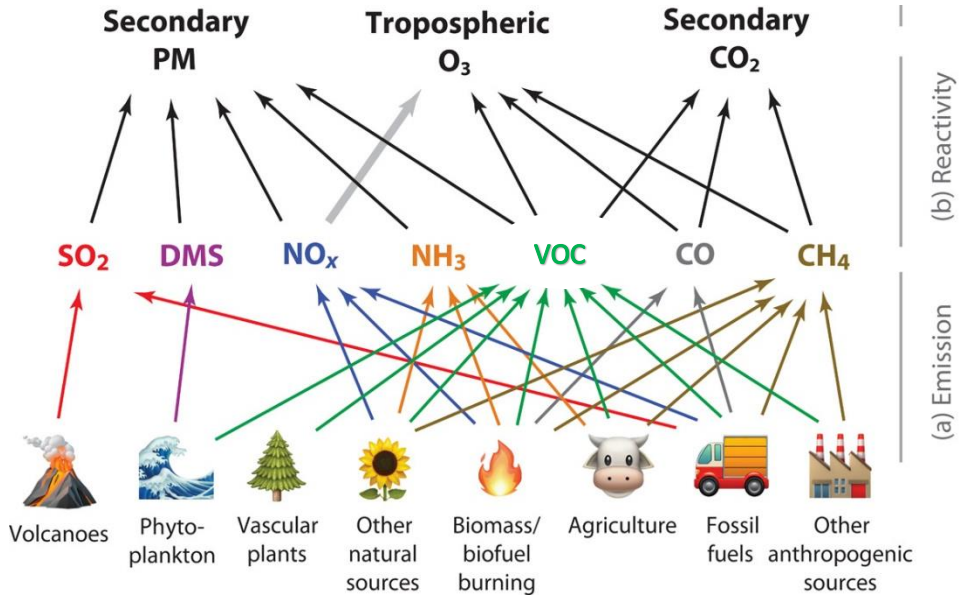

Figure 1.8. The sources of key reactive emissions into the atmosphere that lead to secondary products of interest for air quality (Adapted from Heald & Kroll, 2020).

1.2.2. Primary air pollutants

A relatively large number of pollutants belong to the group of pollutants that are directly emitted in the air. These compounds are presented in the lower part of Figure 1.8.

Primary air pollutants can have multiple different sources varying from volcanic activity to fuel burning or agricultural activities. The most important pollutants directly emitted in the troposphere are: sulphur dioxide (SO_2), dimethyl sulphide (DMS), nitrogen oxides (NO_x), ammonia (NH_3), volatile organic compounds (VOCs), carbon monoxide (CO), and methane (CH_4) (Heald & Kroll, 2020).

SO_2 is emitted during the combustion of sulphur-containing fossil fuels, like coal, oil and diesel, or other sulphur-bearing materials. Furthermore, SO_2 is a natural by-product of volcanic activity. This compound can form secondary pollutants once emitted in the air. It can be slowly oxidized to aerosols (sulphates) or form particulate matter[5] (PM) and acid rain (Miller, 2015). Prolonged exposure or elevated concentrations of SO_2 can cause respiratory problems and irritations of the airways (Brown et al., 2003).

DMS is a compound with the chemical formula $(CH_3)_2S$. It is emitted over the oceans by phytoplankton and can also be produced naturally by bacterial transformation of dimethyl

[5] Particulate matter is a complex mixture of extremely small particles and liquid droplets (aerosols).

sulfoxide (DMSO). Just like SO_2, DMS can form PM once emitted into the atmosphere (Keller et al., 1989).

The nitrogen oxides mainly include nitrogen monoxide (NO) and nitrogen dioxide (NO_2) and can therefore be generally written as NO_x. This group of primary air pollutants is dominant in the upper troposphere and plays a key role in the formation of tropospheric ozone and the hydroxyl radical (OH) in the presence of sunlight, water vapor, and CO or VOCs, (more details on that in section on secondary pollutants; section 1.2.3.) (Haagen-Smit & Fox, 1954). NO_x gases are formed during combustion whenever nitrogen (N) is present. This can be organic N present in the fuel of motor vehicle engines or even N as we know it in the air. NO_x gases can also be produced from lightning via a photochemical reaction, representing a significant amount of the global tropospheric NO_x (Murray, 2016; Schumann & Huntrieser, 2007). Considering indoor pollution, NO_2 is a toxic compound in terms of human health causing respiratory problems and airway irritations if present at elevated concentrations (Kasuga, 1989).

NH_3 is a major air pollutant mainly resulting from agricultural activity. This includes NH_3 emissions from livestock and NH_3-based fertilizer applications. Other sources come from industrial processes, motor vehicles, plant decomposition and biomass burning. It can also be found in trace quantities in nature, for example under the form of natrium salts in for example rain water (Zhu et al., 2015). Gaseous ammonia reacts with other pollutants in the air to form fine particles of ammonium salts which can affect human breathing (Kasuga, 1989).

The group of volatile organic compounds (VOCs) contains thousands of organic chemical compounds which can evaporate under normal atmospheric conditions of temperature and pressure. VOCs are therefore frequently defined by their boiling point. According to the European Union directive of 2004, a VOC is any organic compound having an initial boiling point less than or equal to 250°C measured at a standard atmospheric pressure of 101.3 kPa (European Union Publications Office, 2019). VOCs include aromatic hydrocarbons, aliphatics, aldehydes, ketones, ethers, acids and alcohols. By convention, CO_2, CO and CH_4 are excluded from this list. VOCs are important tropospheric ozone and CO_2 precursors and mainly result from natural emission, like forest fires and the transformation of biogenic precursors. However, the anthropogenic sources of VOCs are on a rise and have become important contributors to their emission. Typical examples are petrochemical activities, industrial burning of fossil fuels, but also different kinds of road and airway traffic and chemical and industrial processes like mining, water heaters and boilers, paint manufacturing and even agricultural pesticides (Montero-Montoya et al., 2018). Possible health effects of VOCs can include airway irritation,

liver or kidney damage, general dizziness, nausea and headache which mainly depends on the toxicity and characteristics of the considered VOC (Shuai et al., 2018; Wu et al., 2012).

CO is another important air pollutant that is emitted during the incomplete combustion[6] of carbon-containing fuels and biomass. Especially vehicle transport is a large contributor to the anthropogenic emission of CO. As CO is also an intermediate in the degradation of other compounds (e.g. CH_4), this species can also be seen as a secondary pollutant. Moreover, CO is an important tropospheric ozone and CO_2 precursor (see section 1.2.3). High indoor concentrations of CO have the ability to replace oxygen that is carried around in the blood thereby reducing the amount of oxygen reaching our cells and fuel them (Rose et al., 2017).

CH_4 has numerous anthropogenic sources, including energy production, such as natural gas and coal, leakage from mining, storage and transport, but also livestock and rice cultivation. Wetlands, termites and biomass degradation naturally contribute to CH_4 production (Heilig, 1994). Beside its role as a major greenhouse gas, it is also a precursor of tropospheric ozone via oxidation by OH and in addition also serves as a precursor for CO_2. Because of its relative long lifetime (± 12 years) CH_4 can reach the stratosphere.

1.2.3. Secondary air pollutants

Although NO_2 and CO were classified as primary pollutants, they can also be seen as secondary pollutants because of their involvement as an intermediate in chemical reactions. PM also belong to this group of air pollutants. However, the main tropospheric secondary pollutants are CO_2 and tropospheric ozone.

The concentration of tropospheric ozone is governed by several chains of reactions and down-mixing of stratospheric ozone.

The main source of tropospheric ozone is via the photolysis of NO_2 and strongly depends on other chemical reactions including NO and VOCs. NO_2 contributes to ozone formation via the following reaction:

$$NO_2 + h\nu \rightarrow NO + O \quad (3)$$

$$O_2 + O \rightarrow O_3 \quad (4)$$

[6] Incomplete combustion entails only a partial urning of a fuel. This generally happens when there is an insufficient amount of oxygen supply.

On the other hand, NO can directly destruct ozone as follows:

$$NO + O_3 \rightarrow NO_2 + O_2 \quad (5)$$

Both reactions are in competition and the actual ozone formation will depend on the ratio of NO_2 and NO concentrations $[NO_2]/[NO]$ (Bozem et al., 2017). An important factor influencing this balance is the VOCs oxidation. Similar to CO, VOCs are a target of OH oxidation. The degradation of VOCs by oxidation leads to the formation of NO_2 (source of O_3) while NO (sink for O_3) is destructed. This means that the production of ozone is favoured by this process.

However, the tropospheric O_3-NO_x-VOC-HO_x chemistry is in reality more complex than that. The net production of tropospheric ozone eventually depends on the initial amount of NO_x and VOCs concentrations present in a certain area. Maximum ozone concentrations are observed in regions where both NO_x and VOC concentrations are high. This is specifically the case in suburb and rural regions (Zong et al., 2018). As shown in Figure 1.9., warmer urban air rises in the troposphere and moves horizontally in the direction of the suburban regions, carrying important air pollutants. This is also known as the urban plume.

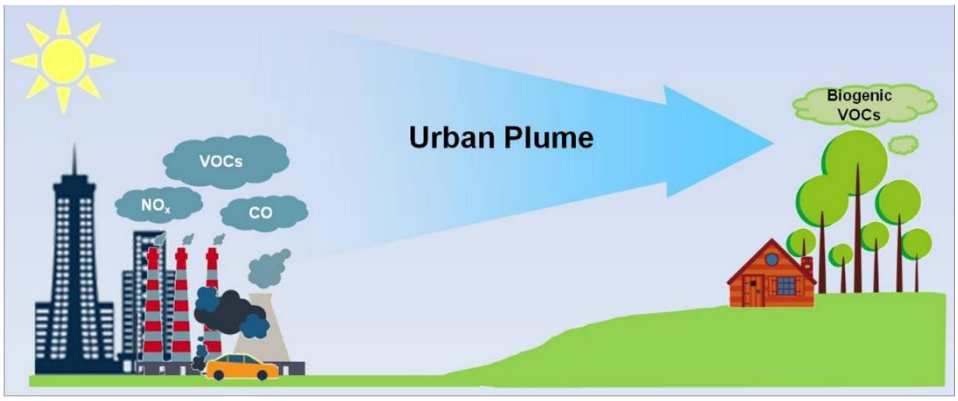

Figure 1.9. Horizontal transport of important urban air pollutants towards suburban regions. [Zong, 2018]

Figure 1.10. is an ozone isopleth diagram[7] illustrating the tropospheric ozone dependence on NO_x (in ppm) and VOC (in ppm carbon (C)) concentrations. In rural areas and suburbs downwind of centre cities, characterized by high VOC/NO_x ratios, it is seen that lowering NO_x concentrations either at constant VOC concentration or in conjunction with lowering VOCs results in lower peak concentrations of ozone. In Figure 1.10. this is specified as the NO_x limited region. We see that the maximum ozone concentration can be reached when the NO_x and

[7] Isopleths are lines of constant value. Each point on a particular isopleth represents the same ozone concentration.

VOCs concentrations are both high. At lower VOC/NO_x ratios (VOC limited region on the figure), lowering VOCs at constant NO_x results in lower peak ozone concentrations. However, the reduction of NO_x concentration in a VOC limited region leads to an increase in ozone production. These low VOC/NO_x ratios are observed in highly polluted urban areas (National Research Council, 1991).

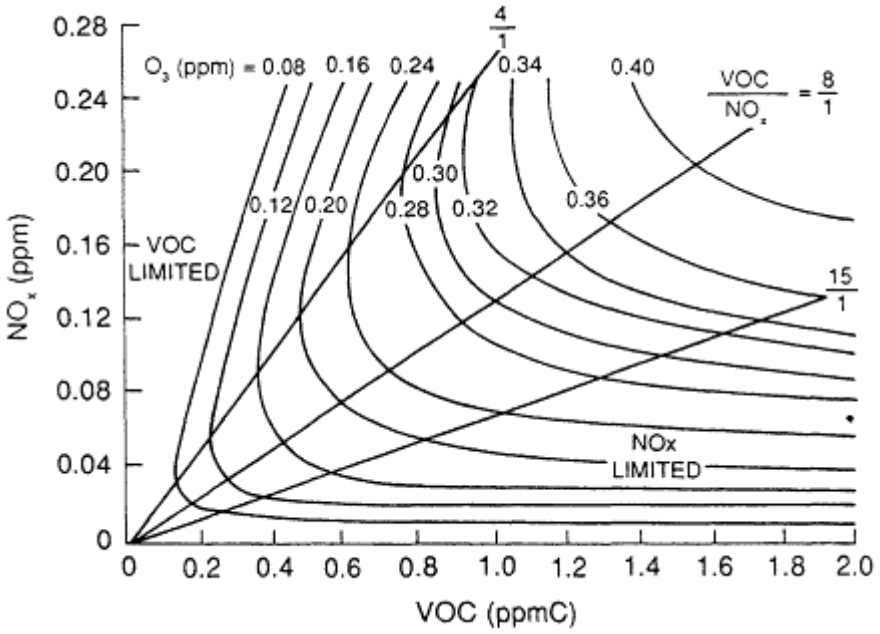

Figure 1.10. Ozone isopleth diagram showing the effect of reducing initial VOC and NOx concentrations on the peak ozone concentrations. From (National Research Council, 1991).

In addition to the O_3-NO_x-VOC-HO_x chemistry, tropospheric ozone can also be formed via other processes. In section 1.1.7 it was already explained how OH contributes as an important oxidizer and sink of several compounds, including CO. A series of chemical reactions following this oxidation eventually lead to the formation of tropospheric ozone and can be written as follows:

$$CO + OH \rightarrow CO_2 + H \quad (6)$$

$$H + O_2 + M \rightarrow HO_2 + M \quad (7)$$

$$NO + HO_2 \rightarrow NO_2 + OH \quad (8)$$

$$NO_2 + h\nu \rightarrow NO + O(^3P) \quad (9)$$

$$O(^3P) + O_2 + M \rightarrow O_3 + M \quad (10)$$

Balance: $CO + 2O_2 \rightarrow CO_2 + O_3$ (11)

Note that this chain of reactions is catalysed by the HO_x (OH, HO_2) and NO_x species (NO, NO_2). This means that a sufficient amount of NO_x needs to be present in the troposphere in order to make these reactions happen. As mentioned earlier, NO_x emission mainly results from human activities so tropospheric ozone production via these reactions mainly take place at high pollution regions (urban and industry regions).

In contrast, regions with insufficient NO_x concentrations will host the next chain of reactions, starting with the oxidation of OH:

$$CO + OH \rightarrow CO_2 + H \quad (12)$$

$$H + O_2 + M \rightarrow HO_2 + M \quad (13)$$

$$O_3 + HO_2 \rightarrow 2O_2 + OH \quad (14)$$

Balance: $CO + O_3 \rightarrow CO_2 + O_2$ (15)

These reactions result in a net destruction of ozone, contrary to the previous series of reactions.

There are still some other compounds that are included in the formation and destruction of tropospheric ozone as for example CH_4 (production of ozone via oxidation by OH). Therefore, it can be generally stated that the abundance of tropospheric ozone is largely controlled by the balance between chemical production and destruction. Stratospheric intrusions of ozone (source) and dry deposition (sink) only contribute to the margin.

1.3. Included tropospheric air pollutants

In this study, we focused on a selection of tropospheric air pollutants retrieved from the Jungfraujoch station. The included compounds are good proxies of air quality and are mostly related to biomass and/or fossil fuel combustion, and oil and gas production. These compounds, together with their lifetime and main sources and sinks are listed in Table 1.2.

Compound	Chemical formula	Lifetime	Main sources	Main sinks
Acetylene	C_2H_2	± 14 days	Biomass burning, fossil fuel combustion	Oxidation by OH
Ethylene	C_2H_4	2 – 4 days	Biomass burning, crude oil and natural gases	Oxidation by OH
Ethane	C_2H_6	2 - 6 months	Biomass burning, biofuel combustion, leakage of the natural shale gas	Oxidation by OH
Methane	CH_4	12 -15 years	Wetlands, termites (natural) Natural gas leak, livestock, rice paddies	Oxidation by OH, transport to stratosphere
Methanol	CH_3OH	± 19 days	Natural gas and coal, plants	Oxidation by OH
Formaldehyde	H_2CO	a few hours	Biomass combustion, volcanic emission Fuel combustion, industrial emission	Photo-oxidation, oxidation by OH
Hydrogen cyanide	HCN	2 – 4 months	Biomass burning	Ocean uptake
Formic acid	HCOOH		Venom of bee and ant stings, forest emissions Industrial (produced from methanol)	Decomposition by heat and acids
Carbon monoxide	CO	± 2 months	Incomplete combustion of fossil fuels and biomass, oceans, hydrocarbon oxidation	Oxidation by OH, soil uptake
Ammonia	NH_3	few hours – a day	Plants, rain droplets Agricultural and industrial activity	Reaction with acids to produce PM
Ozone	O_3	± 1 month (troposphere)	Transport from stratosphere Chemical production	Chemical loss, dry deposition

Table 1.2. Overview of the included tropospheric air pollutants, retrieved at the Jungfraujoch station.

2. Data retrieval at the Jungfraujoch Observatory

The geophysical data analysed in this work were already reduced. Still, a brief discussion on how they were retrieved from the infrared solar absorption observations routinely recorded at the Jungfraujoch Observatory is given in this second chapter.

2.1. The International Scientific Station of the Jungfraujoch

The Sphinx Observatory is part of the International Scientific Station of the Jungfraujoch (ISSJ) and is located in the Swiss Alps (46.55° N, 7.98° E) (see Figure 2.1.). Its ideal location gives researchers the privilege to operate under excellent observation conditions. Since the water vapour abundance is about 20 times lower at this Swiss region compared to sea level abundances, the air is notably dry. Furthermore, the air above the ISSJ is extremely clean, only harbouring minimal concentrations of local pollutants as there are no large industries present in a radius of 20 km. Because of its altitude (3580 m above sea level), the station is mostly active in the free troposphere.

Figure 2.1. The Sphinx Observatory in the Swiss Alps.

The observatory plays an important role in conducting long-term atmospheric experiments. A range of atmospheric parameters is collected, including trace gases and aerosols concentrations together with meteorological and solar data. Techniques used for the retrieval of these parameters include solar infrared, microwave and UV spectroscopy, GPS receivers, mass spectrometry and many others.

The Infrared Group of Atmospheric and Solar Physics (GIRPAS; see http://labos.ulg.ac.be/girpas; Institute of Astrophysics and Geophysics, ULiège) operates the solar infrared spectrometer of the observatory for a range of long-term experiments. Atmospheric species that are routinely monitored, in terms of vertical total and partial abundances, with the infrared spectrometer are fundamental gases covered by the Kyoto or Montreal Protocol (see Table 2.1.).

More than 35 atmospheric constituents are constantly monitored		
Greenhouse gases	H_2O, CO_2, CH_4, N_2O, CF_4, SF_6	**Kyoto Protocol and the Paris Agreement**
Stratospheric ozone-related	O_3, NO, NO_2, HNO_3, $ClONO_2$, HCl, HF, COF_2, CFC-11, CFC-12, HCFC-22, HCFC-142b, CCl_4, CH_3Cl	**Montreal Protocol** on ozone depleting substances
Air quality, biomass burning, oil and gas production…	CO, CH_3OH, C_2H_6, C_2H_2, C_2H_4, HCN, HCHO, HCOOH, PAN, NH_3	**Europe's eyes on Earth (Copernicus program)**
Others	OCS, N_2, isotopologues[8]	Various applications

Table 2.1. Target gases currently retrieved from the FTIR monitoring program conducted at the Jungfraujoch station.

The first activities of the Liège group at the ISSJ date back to the 1950's when Prof. M. Migeotte and his team performed the first solar infrared observations. The instrument used was a 1 m focal length grating spectrometer[9] that was able to record absorption bands of CO_2 and CH_4 (Migeotte, 1950; Nielsen, 1952). A second grating spectrometer replaced the first instrument in 1958. It was in operation until 1989, to study the solar photosphere and also, later, the Earth's atmosphere. In 1974, the first Fourier Transform Spectrometer (FTS), also called the

[8] an isotopologue is a molecular twin that differs from the original molecule in the isotopic composition only; for example, $^{13}C^{16}O$ and $^{12}C^{18}O$ are isotopologues of the most abundant $^{12}C^{16}O$.
[9] An instrument that uses a diffraction grating to disperse light into a spectrum.

Home-built FTS, was installed at Jungfraujoch. This instrument was built in Liège and operated together with the grating spectrometer to record infrared solar absorption spectra. In 1989, the grating spectrometer was replaced by a Bruker IFS-120 HR. This FTS and the Home-built instrument were regularly operating together until 2008, when the homemade instrument was decommissioned. There are numerous examples of combined and consistent time series, e.g., time series of morning and twilight observations of O_3 and NO_2 total column amounts derived from the two Fourier Transform Infrared (FTIR) instruments since 1990 (Cui et al., 2011; Hendrick et al., 2012). Since 2008, there is a complete remote control of the Bruker spectrometer designed and implemented by the team of Servais (cfr https://orbi.uliege.be/handle/2268/64605).

Regular operations with these instruments helped to build the largest FTIR database available worldwide. Both FTIR spectrometers of ULiège are affiliated to the Network for Detection of Atmospheric Composition Change (NDACC; see http://www.ndacc.org). The NDACC is a network of more than 70 ground-based remote-sensing research stations worldwide which also includes balloon sounding activities.

2.2. Data retrieved from infrared spectra

2.2.1. The principle behind infrared spectroscopy

Electromagnetic radiation can interact with atmospheric constituents. Depending on the type of molecules, atoms or particles, a specific absorption spectrum is generated. This principle is involved in molecular spectroscopy where these spectral lines give information on the structure and composition of the materials present in the considered sample. This has to do with the fact that material only absorbs specific wavelengths of electromagnetic radiation depending on its structure. Infrared spectroscopy is a part of molecular spectroscopy which only includes infrared radiation. This type of radiation represents the region of the electromagnetic radiation spectrum with wavelengths between ~1 and 13 µm, or 600 and 4400 cm^{-1}. These amounts of energy are sufficient to cause vibrational and rotational transitions, which are specific to the active molecules. Regarding vibration, this means that molecules, depending on their composition and structure, can vibrate in different ways when absorbing the desired amount of energy. All the possible vibrational motions of a molecule can be described in terms of fundamental modes (also referred to as normal modes of vibration), which contains two categories of vibration: stretching and bending modes. The stretching modes refer to a

variation of the bonding length between the atoms, whereas the bending modes involve the change of bonding angles in the molecule. To give an example, Figure 2.2. illustrates the different vibrational modes of H_2O where each mode has its own specific frequency of vibration ν which corresponds to a wavenumber[10] (expressed in cm^{-1}). A condition for a molecule to be active in the infrared is that a dipole moment must be generated. This means that diatomic molecules such as H_2 are not active in the infrared and will not show any absorption lines in the spectrum. Note that here we are discussing about allowed dipolar transitions. There are also forbidden transitions like the quadrupolar IR emission of H_2 at 2.2 µm.

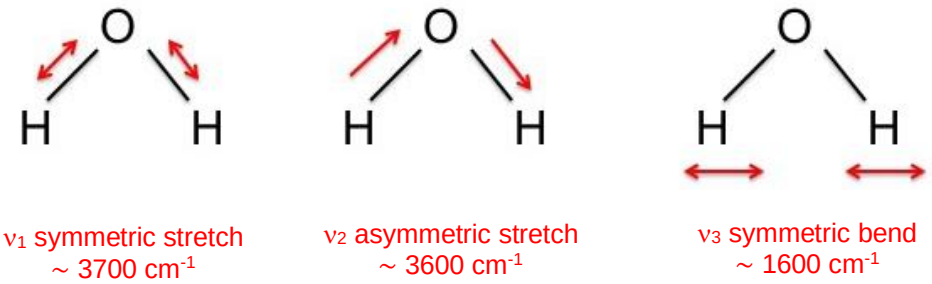

Figure 2.2. The three fundamental modes of vibration for water. (Richard Jones, utexas.edu)

When the frequency of the incoming radiation matches the vibrational frequency of a molecule, this radiation will be absorbed. As the ro-vibrational frequencies of a molecule depend on its structure and composition, they will only be able to absorb radiation with these specific values. The absorbed energy is consumed and thus missing from the original infrared beam. In spectroscopy, the infrared spectrum represents the fraction of radiation transmitted (so not absorbed) through the atmosphere as a function of the wavelength. This way, an atmospheric infrared spectrum can perfectly tell which and how much molecules are present in the "sample". Note that it also depends on the pressure and temperature of the sample. IR emission spectroscopy is also in use in remote sensing of atmospheric composition (Earth and much more).

2.2.2. Fourier-Transform InfraRed Spectrometer: spectra generation

In order to detect and obtain information on different atmospheric compounds with infrared spectroscopy, a ground-based Fourier-Transform InfraRed Spectrometer can be used. The set-up of this spectrometer is based on the principle of a Michelson type interferometer (see

[10] Wavenumber is the number of waves in a distance 2π.

Figure 2.3.). This interferometer contains two mirrors: a moving mirror and a fixed mirror together with a semi-reflector beam-splitter.

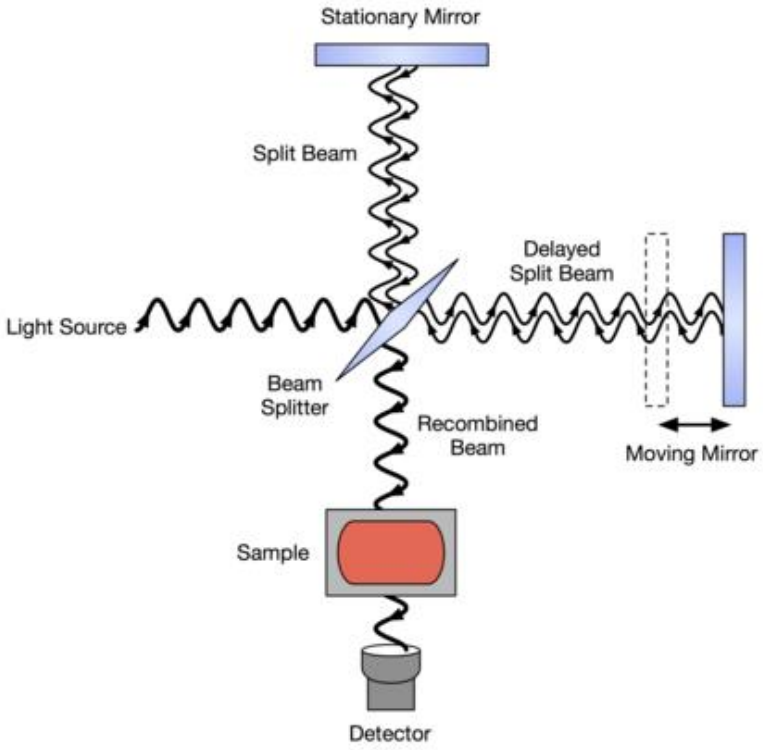

Figure 2.3. Optical configuration of a Michelson Interferometer. *(Al-Saeed & Khalil, 2010)*

Incoming solar radiation is conducted to the instrument entrance via a sun-tracker. The incident light falls on the beam-splitter where one half of the beam is transmitted and the other half reflected. Each of these beams of equal intensity are directed towards one of the two mirrors which reflects the beams back to the beam-splitter. Here, the two separate beams recombine causing interference. The recombined light beam goes through the atmospheric sample and is focused on a detector. The signal detected is the light intensity of the combined beams versus the optical path difference (as the second mirror is constantly moving) and is represented in an interferogram. A maximum signal displays when the paths of both beams have the same length because of constructive interference (this is also called the zero optical path difference). The mid-IR is covered by five optical filters of typically a few tens up to 30 wavenumbers and several consecutive scans are combined to produce an interferogram. This is done in order to increase the signal-to-noise ratio. The actual spectrum that is acquired in the end is the result of applying a Fourier-transform on the interferogram.

2.2.3. Analysis of the spectra

After selecting the narrow range micro-windows from the spectra, a specific code is used to determine the vertical abundances and total columns of the atmospheric gases. For this purpose, the SFIT algorithm has been developed by C.P. Rinsland (NASA-Langley), B.J. Connor (National Institute of Water and Atmospheric Research, Lauder, New Zealand) and J.W. Hannigan (National Center for Atmospheric Research, NCAR, Boulder, CO) (version currently in use is SFIT-4 v0.9.4.4). This specific code generates a synthetic spectrum in a given spectral range and fits it to the recorded FTIR spectrum using an iterative process. This process is illustrated in Figure 2.4. The synthetic spectrum is generated from spectroscopic line parameters and an atmospheric model. The atmospheric model includes pressure and temperature vertical distributions (p-T profiles), a vertical layering scheme of the target and a priori mixing ratio profiles for the target and interfering species. p-T profiles are provided by meteorological centers (e.g. the National Centers for Environmental Prediction; NCEP) and are based on satellite observations. The vertical distribution of the target is based (in this case) on a 40-year simulation performed at NCAR. Once the synthetic spectrum is generated, it will be processed by the SFIT-4 code. The code will start looping (blue arrows) and adjusts the synthetic spectrum until best fit agreement is obtained with the recorded spectrum. This is done by calculating the difference between the two spectra followed by the scaling of the included parameters bringing this difference to a minimal value. In the end, when there is a best match between these two spectra, all data is converged (green arrow) to produce vertical profiles of the gases. Total columns are then retrieved from these vertical profiles (Hase et al., 2004; Rinsland et al., 1998).

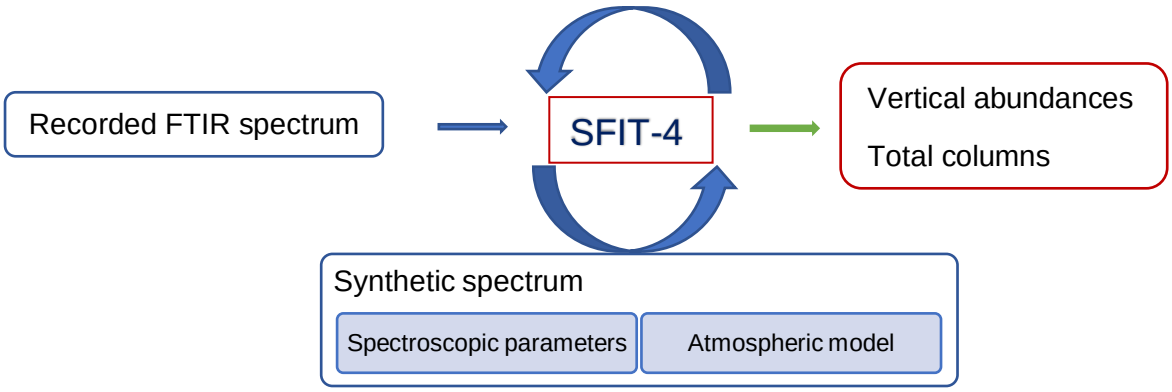

Figure 2.4. Schematic representation of the determination of geophysical parameters using the SFIT-4 algorithm.

This iterative process of fitting a synthetic spectrum to the recorded one is illustrated in Figure 2.5. using C_2H_6 as an example. In this figure, A shows the residuals of the comparison between the recorded spectrum and the synthetic spectrum before any iteration has been done, hence assuming the a priori profiles for the target and interfering species. Here, the fitted root mean square (FITRMS) is equal to 2.66%. In panel B, the recorded (green) and synthetic (red) spectrum are shown before the iteration process. C displays the fitting residual after convergence (here, 6 iterations were needed). The FITRMS is now set at 0.12%. Panel D, represents the recorded and fitted spectra which are now hard to distinguish. In E, the a priori and retrieved profiles for water vapour and ethane are shown with two horizontal dedicated axes. While also fitted, ozone is not shown in Frame E as it would require yet another horizontal scale, and is a minor absorber in the three intervals.

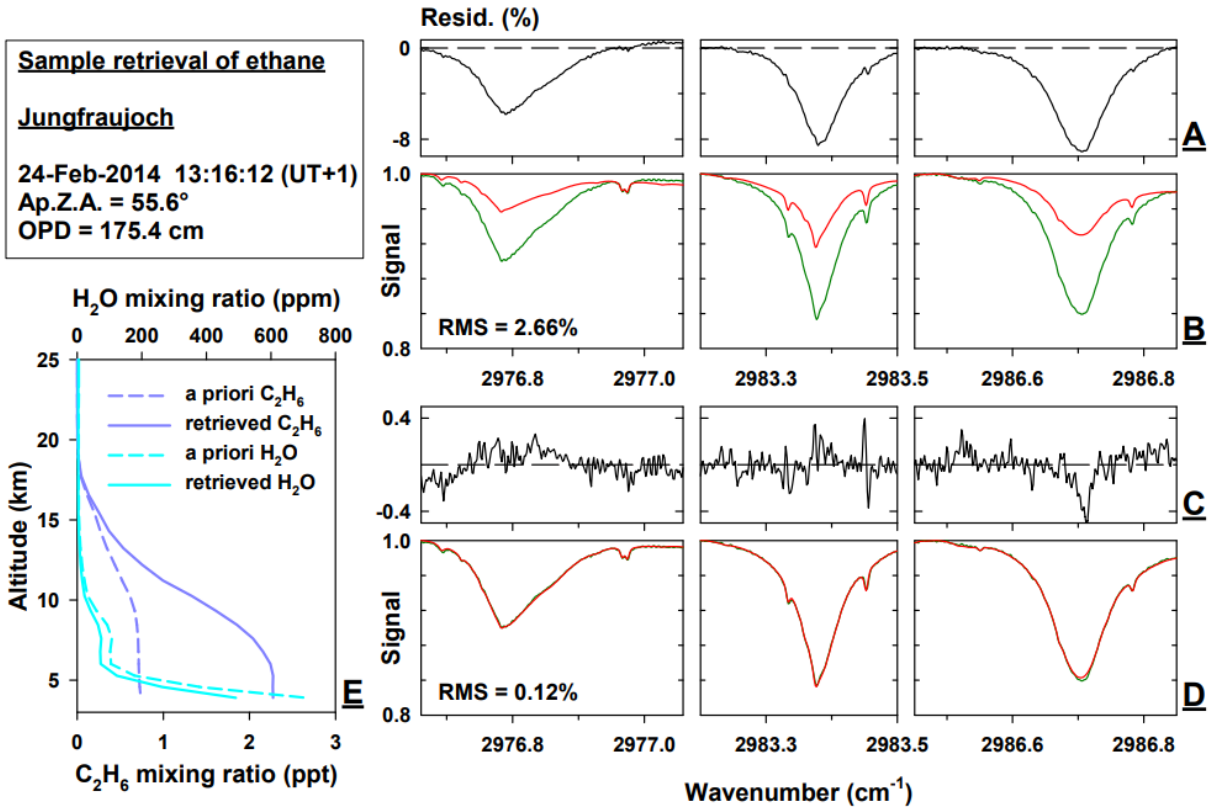

Figure 2.5. Sample fit for ethane (C_2H_6) retrieved at Jungfraujoch using 3 micro-windows (GIRPAS).

3. Construction of reference multiyear time series

Within the context of the covid-19 pandemic and related prolonged lockdown period it is interesting to study the abundances of multiple air pollutants in 2020 and to compare them with reference levels based on the measurements available for the last decade(s). The construction of a climatological model per species is thus needed to build a representative data set. In this section, a description on this is given together with an interpretation of the related results.

3.1. Raw data processing

3.1.1. Data selection and filtering

The raw unfiltered FTIR datasets directly retrieved from the Jungfraujoch were made available for the purposes of the master's thesis. The outputs of the FTIR measurements are time series of vertical profiles of the different monitored species. Measurements at the observatory were performed on a daily basis over several years (CO for example dates back to 1984). At this moment, there is no data available for year 2021 because the Bruker spectrometer has been down since mid-December last year due a technical problem. The related parameters for each species were combined in tables from which further data processing was performed. As mentioned before, this study focused on a selection of the relevant species among those listed in Table 1.2.

The vertical profiles were derived in 41 successive layers homogeneous in terms of temperature, pressure and mixing ratio for the target species. These layers range between the site altitude of 3.58 km and 120 km. The vertical mixing ratios are expressed in parts per volume (ppv) indicating the fraction of a given molecule with respect to the total number of molecules in a specific layer of air. Mixing ratios with negative values (e.g., resulting from noise in the spectrum) were excluded from the dataset.

The total column amount of each species, in molecules/cm², corresponds to the total number of molecules of a given gas contained in a vertical column of a cm² area, summed over the whole atmosphere, practically from the site altitude up to 120 km. Data removed from the list consisted of total column concentrations not fulfilling certain criteria. First, total column concentrations with too small values of the degrees of freedom for signal (DOFS; an objective measure of the information content or number of independent pieces of information available in a given measurement) were excluded by removing the lower 5% values of the

measurements. Second, the same principle was applied to the FITRMS values but here the upper 5% was filtered out, corresponding to poor fitting residuals (see Figure 2.5.). Finally, total columns for which convergence of the SFIT-4 software was not reached (CVFLAG indicated as “False”) were removed from the dataset.

3.1.2. Calculation of monthly means

After selecting the useful data, monthly means of the concentrations were calculated for each individual species over a certain number of consecutive years. As all included gases, except for O_3, are mostly lying in the troposphere, it was assumed that taking the monthly means of the total columns would be relevant. Since O_3 is primarily a stratospheric gas, the total columns will possibly only marginally respond to the lockdown. Therefore, mixing ratios at tropospheric altitude were considered for O_3 instead of total columns by summing up all the levels from the lowermost partial column to about 10 km altitude. This approach is consistent with some other studies (Gardiner et al., 2008; Vigouroux et al., 2015).

The time period this study focused on included the last 10 years (excluding year 2020) starting from January 2010 to December 2019. Only for tropospheric O_3 the data for the last 20 years was used (January 2000 – December 2019). Because of the thesis’ time restrictions a 10-year time period seemed to be the best option as it is easier and less-time consuming to handle the data. When considering a larger period of time, it becomes more complicated to normalise the data for the trend since there are possibly more fluctuations in concentrations. Although it is easier to work with less data, it has to be kept in mind that the results become less robust. However, for the purposes of this master’s thesis it was assumed that looking at the concentrations over a 10-year period would suffice. Furthermore, for more than half of the selected species for this study there was no data available for a longer period of time. For tropospheric O_3, it was decided to look into the O_3 concentrations over a 20-year time period (from January 2000 to December 2019), in analogy with the study of Steinbrecht et al. (Steinbrecht et al., 2021).

3.2. Trend analysis

Long-term measurements of different compounds present in the atmosphere can often be characterised by an increasing or decreasing linear trend over time. Before comparing the data of 2020 to the 10- or 20-year time series for each species it is important to determine if each

individual species has a statistically significant long-term trend and to account for that if needed.

3.2.1. Bootstrap resampling trend analysis

As FTIR data typically show intra-annual variations (seasonal variations) a basic linear trend model might not provide robust or representative results (fitting a straight line using for example the least squares criterion). The distance from the datapoint to the linear fit depends on the time of the year and is often non-normally distributed. Therefore in this study, a bootstrap resampling trend analysis was performed on each individual species using a Matlab script file developed by A. Forbes at the National Physical Laboratory (NPL) (Gardiner et al., 2008). This method accounts for seasonal variations and excludes the assumption of normality providing good fits even in the presence of large gaps in the data (Gatz & Smith, 1995) or of significant outliers. The seasonal variability is modelled in terms of a Fourier series (here: 3rd order), i.e.:

$$V(t,b) = c_0 + c(t-t_0) + b_1\, cos2\pi(t-t_0) + b_2 sin2\pi(t-t_0) + b_3 cos4\pi(t-t_0) + b_4 sin4\pi(t-t_0) + b_5 cos6\pi(t-t_0) + b_6 sin6\pi(t-t_0) \quad (16)$$

where c_0 is the abundance at the reference time t_0 (in years) for the linear component, and c is the annual trend. The function F fitted by the bootstrap tool combines a seasonal modulation and a simple linear change, i.e.:

$$F(t,a,b) = at + V(t,b) \quad (17)$$

where a is the annual trend. A next step included the fitting of the model function $F(t,a,b)$ to the data (t_i, M_i) where t_i represents the fraction of the year (e.g. 2005.500 refers to the middle of the year 2005) and M_i is the corresponding total column:

$$\sum_{i=1}^{m} \left(M_i - F(t_i,a,b)\right)^2 \quad (18)$$

From this, the initial fit can be determined (a_0 and b_0) from which residual deviations are calculated, i.e.:

$$\mathrm{R}_{i,0} = M_i - F(t_i, a_0, b_0) \quad (19)$$

A new dataset $\{t_i, M_{i,q}\}$ is generated using $R_{i,q}$ which is randomly sampled from the dataset $\{R_{i,0}\}$:

$$M_{i,q} = F(t_i, a_0, b_0) + R_{i,q} \quad (20)$$

Next, the model is refitted to this data giving a_q and b_q. This is then repeated 50,000 times (q = 1, …, 50,000) generating a set of trend results $\{a_q\}$ and seasonality parameters $\{b_q\}$ ((Gardiner et al., 2008).

3.2.2. Statistical analysis

The output of the bootstrap resampling trend analysis provides a value for the annual trend (in molecules cm^{-2} $year^{-1}$) together with the 2.5 and 97.5 percentiles specifying a 95% confidence interval associated with this trend value. For the statistical analysis the null hypothesis can be defined as follows: “there is no statistically significant linear trend for the data” or in other words, the gradient of the linear trend is not different from zero. This means that if the value zero is not included in the 95% confidence interval, this hypothesis is false and the considered species is associated with a statistically significant trend over the period of time considered. Table 3.1. includes the compounds selected for this study with their mean trend ± standard deviation (SD; 2-sigma level) computed by the bootstrap tool, the mean abundance and annual trend value ± SD (2-sigma level) in %. The mean abundance was used to compute this relative trend. The period for which the annual trend was calculated for each molecule is also given in this table. The annual trend values in bold indicate that this trend is statistically significant.

	Period (years)	Mean trend ± 2 SD *	Mean abundance*	Annual trend ± 2 SD (as % of the mean abundance)
C_2H_2	10	-1.26E+13 (±1.13E+13)	1.22E+15	**-1.03 (±0.93)**
C_2H_4	10	-2.46E+12 (±1.19E+13)	1.47E+14	-1.68 (±8.07)
C_2H_6	10	9.83E+13 (±7.33E+13)	1.05E+16	**0.93 (±0.70)**
CH_4	10	1.17E+17 (±2.04E+16)	2.47E+19	**0.47 (±0.08)**
CH_3OH	10	6.96E+13 (±1.16E+14)	7.38E+15	0.94 (±1.57)
H_2CO	10	2.26E+13 (±1.30E+13)	1.30E+15	**1.74 (±1.00)**
HCN	10	-2.95E+13 (±2.31E+13)	3.64E+15	**-0.81 (±0.64)**
HCOOH	10	-6.76E+12 (±1.99E+13)	6.66E+14	-1.02 (±2.98)
CO	10	-7.11E+15 (±3.42E+15)	1.06E+18	**-0.67 (±0.32)**
NH_3	10	9.84E+12 (±6.30E+12)	2.06E+14	**5.53 (±3.14)**
O_3	20	-1.40E-10 (±1.99E-09)	6.40E-07	-0.02 (±0.31)

Table 3.1. Annual trend results obtained with the bootstrap resampling trend analysis method. Statistically significant trend values are indicated in bold.
**in molecules/cm² (in ppv for O_3)*

3.3. Detrending the data

Species showing a statistically significant annual trend over the defined period (10 or 20 years) had to be normalised ("detrended") before it can be used for comparison with the 2020 monthly means. This was done for all molecules of Table 3.1. shown in bold. Removing the effect of the trend is of importance since this can significantly influence the potential difference between the subsets of the two different periods, potentially leading to misrepresented results. In order to eliminate the trend, linear regression was applied to normalise the data, using 2019 as a reference. The principle behind this linear regression is that a regression model is fitted to the data (2019 reference in this case) from which the difference between the observed values and the model values is calculated. This is shown in Figure 3.1. using the Jungfraujoch CH_4 monthly means as an example. This figure gives both observed CH_4 monthly mean total columns (in molecules/cm²) and normalised total columns as a function of the average date of the corresponding month. The linear trend derived from the monthly means before normalising increased with 0.47% (±0.08%) between January 2010 and December 2019 (orange line Figure 3.1.).

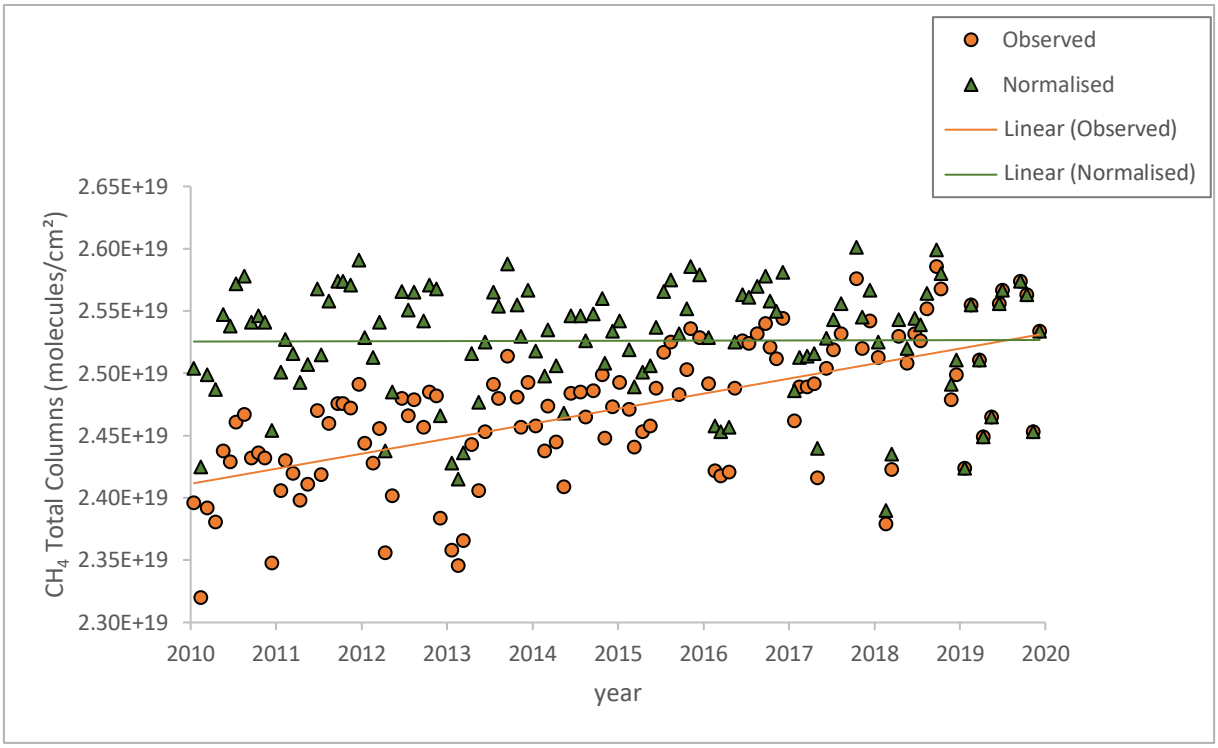

Figure 3.1. Example of detrending monthly means over a 10-year period, here for CH_4. The observed monthly means were normalised using the linear component with the year 2019 as a reference.

3.4. Correction of the data

Before comparing the climatological time series to the 2020 abundances, the computed monthly means and their trend were properly checked. There were two peculiarities observed in the data of two species that needed to be investigated and corrected.

First, in December 2013 the monthly mean value of the NH_3 total columns was noticed to be much higher than the values for the other months over 10 years. More specifically, the 10th of December 2013 had an average total column concentration of more than 17 times the average concentration (mean total column of 3.57E+15 molecules/cm² vs. 2.09E+14 molecules/cm²). This was apparently due to a NH_3 leak caused by a small fridge at the lab used by the scientists to store their lunch and drinks. However, a leak in such a device caused a large increase of the measured NH_3 by the FTIR spectrometer. Since the instrument measured an excess of NH_3 representing the inside air and not the atmosphere above the Jungfraujoch, related datapoints were discarded. In total, 3 measurements showing the increased NH_3 values were removed, all captured on the same day (10-12-2013). The trends of NH_3 datasets with and without the fridge data were compared to see if any changes in the computed trend values (using the bootstrap tool) were present. The calculated trend for the uncorrected data (with the

fridge data) corresponded to +5.32%/yr (±3.35%) compared to +5.53%yr (±3.14%) for the corrected dataset. Both trends were statistically significant.

A second peculiarity was found for the CO time series in the second semester of 2015. The optical filter used for CO was inducing fringing which is the presence of instrument-induced periodic oscillations of spectral transmission resulting from internal optical resonances (Blumenstock et al., 2021). A nearly sinusoidal modulation was *a posteriori* superimposed to the synthetic spectra in order to account for this, for all spectra from 07/2015 until 12/2015. Figure 3.2. shows the effect of the correction where the CO total columns are plotted as a function of the calendar year. In the upper panel of Figure 3.2., the improvement for the fitting residuals (FITRMS) is presented whereas the lower panel shows the CO total columns. The FITRMS and total column values are represented in black and red referring to the dataset with and without correction, respectively. This figure clearly shows that fringing has little effect on the retrieved total columns for CO, a strong absorber. In contrast, the fitting residuals (FITRMS) were strongly affected, causing the rejection of a semester of CO data because of fringing. As explained in section 3.1.1. the data corresponding to the highest 5% of the FITRMS values are indeed filtered out. For this reason, it is preferable to use the corrected dataset.

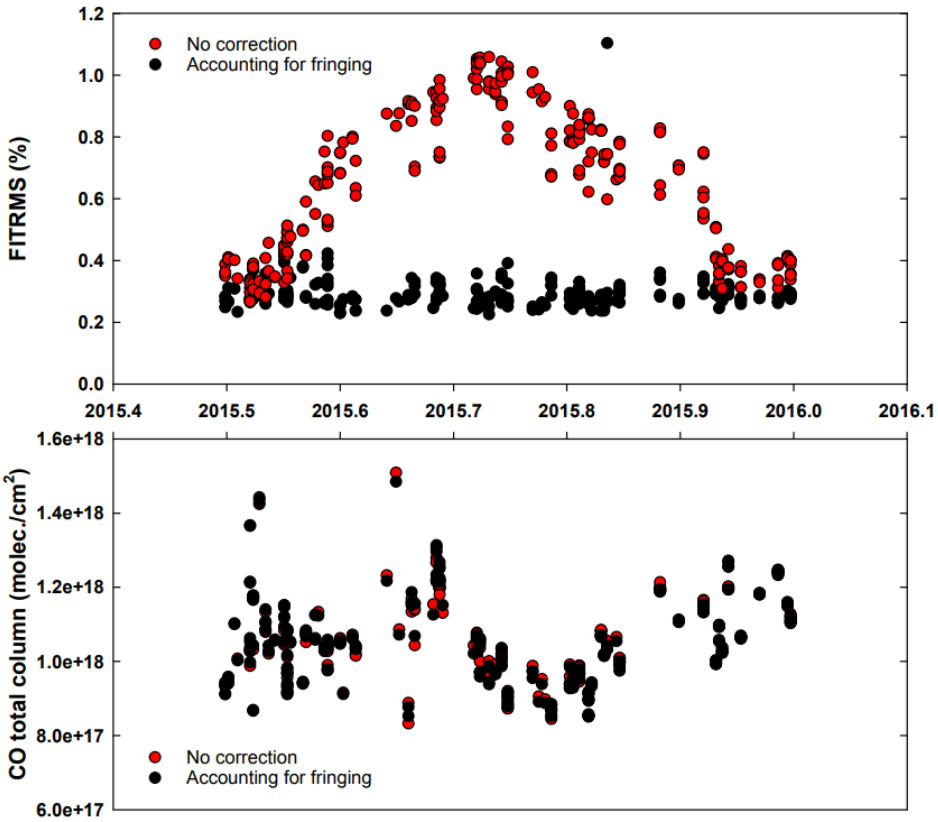

Figure 3.2. GIRPAS quality control figure showing CO data before and after correction for fringing. The FITRMS values (upper panel) and CO total columns (lower panel) are represented as a function of the calendar year.

3.5. Interpretation

3.5.1. Interpretation of the trends

As discussed in section 3.2.2. more than half of the studied species show a statistically significant trend over time (see Table 3.1.). These gases include C_2H_2, HCN, CO (decreasing trend) together with C_2H_6, CH_4, H_2CO and NH_3 (increasing trend).

For C_2H_2, HCN, CO the explanation for their associated negative trend during the last decade possibly lies within the fact that there is a significant reduction in their emission as there is a strong correlation between HCN and CO columns due to their common biomass burning source (C_2H_2 is also produced from biomass burning but this is less dominant).

The evolution of the atmospheric concentrations of CH_4 shows an increase between 2010 and 2019 of 0.47%/yr. The growth slowed down in the 1990s and increased again from the mid-2020s, after a plateau in 2000-2004. Comparison between observations and model data indicates that the exploitation of coal, natural gas and oil are the main causes of this increase, in addition to increased emissions from wetlands. However, the exact reason for the evolution of methane in the past has not yet been completely resolved (Bader et al., 2017; Schaefer, 2019). In addition to this, it was expected to see an increasing trend for H_2CO (1.74%/yr) since the production of this species is strongly influenced by the abundance of CH_4. Through the oxidation of CH_4 by the hydroxyl radical in the troposphere, H_2CO can be generated in only a few seconds (Franco et al., 2016).

According to several studies, a prolonged decrease (-2.7%/yr) was observed for C_2H_6 until 2009 (Simpson et al., 2012). Starting from that year a sharp increase in its trend is dominant which is also confirmed by the outcomes of this study (increase of 0.93%/yr) (Mahieu et al., 2018). The detection of the recently increasing trend is of great importance as C_2H_6 is the most abundant non-methane volatile organic compound. The main cause to explain this increase is related to the oil & natural gas boom in North America (Franco et al., 2016; Helmig et al., 2016). A strong increase in oil prices resulted in the intensification of the shale gas exploitation by the oil industry, making this costly technique profitable (data available on the website of the U.S. Energy Information Administration: https://www.eia.gov/). C_2H_6 has a well-known latitudinal gradient showing a significant increase only present in the Northern-Hemisphere because this is where most emissions take place.

For ammonia, the largest annual increase (5.53%/yr) was observed. This is highly in contrast with the decreasing NH_3 emissions from 1990 to 2012 and small increase of 3% since 2013

reported by the European Environmental Agency (*European Environment Agency (EEA) 2020 Air pollutant emissions data viewer*, 2020). This suggests that meteorological factors need to be taken into account in order to explain this strong contradiction. Exceptional weather conditions including extreme drought and high ambient temperatures of the last years likely explain this high value for the trend (Hari et al., 2020; Van Damme et al., 2020). Also, decreased emissions of SO_2 and NO_x result in less chemical loss of NH_3. However, these explanations are not sufficient to justify this increase in NH_3 over the last decade (van Zanten et al., 2017; Yao & Zhang, 2019).

3.5.2. Interpretation of the seasonal cycles

The seasonal variations give information on which period during the year there is a maximum and minimum value for the total or partial columns. All air pollutants included in this study were characterised by showing seasonal variations during each year. In Figure 3.3. this seasonality is illustrated using HCN as an example giving the HCN total columns as a function of the year (from 2010 to 2019). The blue line show the observed data represented as monthly means accompanied by its trendline which was computed by the bootstrap tool. The seasonal variability is modelled in terms of a Fourier series (shown in green).

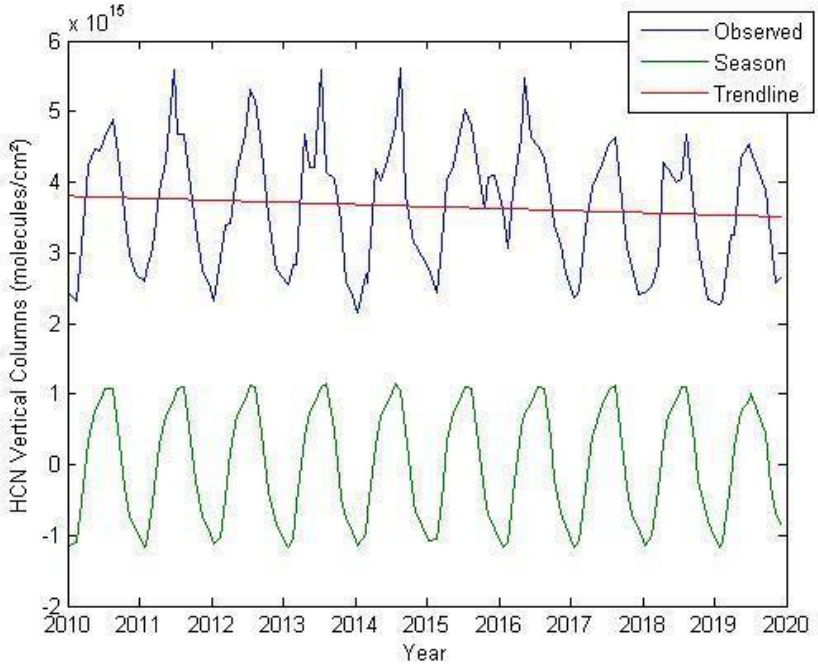

Figure 3.3. Example of the extraction of the HCN seasonal variability in total columns obtained by the bootstrap resampling method.

As illustrated in Figure 3.3., HCN abundance in the atmosphere above the Jungfraujoch is maximal in spring-summer and minimal in the winter. In general, the positions of these maxima and minima differ from species to species and mainly depend on their dominant sources and sinks. In the example of HCN, biomass burning is known to be its most important source, whereas ocean uptake mainly contributes to HCN destruction in the atmosphere (Li et al., 2009). Since the amount of biomass burning is higher during spring-summer time annual peaks in the HCN concentration show up here. However, for some compounds other source and sink mechanisms are dominant. As mentioned in section 1.1.7., the hydroxyl radical (OH) is a major oxidant in the troposphere thereby being a dominant sink of several species. OH is mainly produced during the summer months by sunlight causing lower concentrations of these affected species in this period of the year. C_2H_2, C_2H_4 and CO for example, will behave this way. Emissions because of road traffic barely have seasonal variations since this source is more is almost constant throughout the whole year. This confirms that the variations between species in the seasonality is due to the fact that different species have different types of sources and sinks.

4. Evaluation of the effect of lockdown on the abundance of the included air pollutants

4.1. Defining the lockdown period

Before any conclusions can be drawn from the compared monthly means, it is of importance to find a way to specify lockdown. Officially, lockdown can be defined as a state of isolation or restricted access instituted as a security measure *(Oxford Languages (oup.com))*. Due to the measures taken by most governments worldwide in order to minimise the spread of the covid-19 virus, many countries were in lockdown. However, the specific implemented rules varied mainly depending on the severity of the pandemic at the considered time and location. In general, we can state that human activity was mainly impaired during the first half of the year 2020 when the World Health Organisation (WHO) officially declared a global pandemic on 11 March 2020. This decreased activity can be projected in different measurable effects which can contribute to the construction of a more precise definition of lockdown in the context of the covid-19 pandemic.

One way to address lockdown is to look at CO_2 emissions, as done by (Steinbrecht et al., 2021). Before the year 2020, CO_2 concentrations had known an annual increase of 0.6% over the last decade (Peters et al., 2020). By April 2020, daily CO_2 emissions decreased by -17% compared to the 2019 means, worldwide (Le Quéré et al., 2020). This effect was dominantly attributed to the immediate reduction in energy demand, with surface transport and air traffic as key players. By July 1st, this effect diminished when the government's measures became less strict, although the effect was still minimally present (Liu et al., 2020).

Second, the 2020 lockdown can also be expressed in terms of black carbon (BC) emissions. BC is a component of fine particular matter mainly produced from incomplete carbonaceous fuel combustion. BC has strong health impacts and contributes to global warming: it absorbs a lot of sunlight and reduces the albedo of snow and ice when being disposed on it. Since this pollutant is largely produced from anthropogenic sources, the correlation with the lockdown period can be made. A study of Evangeliou et al. has shown that BC emissions have decreased by 23% in Europe during lockdown in comparison with the previous 5 years during mid-March to April, when the measures were the most strict (Evangeliou et al., 2021).

Another potential way of approaching the concept of lockdown is to study human mobility data. Google and Apple each publish data that reports the mobility of humans in terms of driving, walking and the use of public transport (Google: https://www.google.com/covid19/mobility/; Apple: https://covid19.apple.com/mobility/) (Sannigrahi et al., 2021). This way, a bridge can be

made between the lockdown and emission of air pollutants related to human transport (motorised road traffic). Figure 4.1. shows the Apple mobility report from 13 January 2020 to 19 May 2021, only including the data for driving and public transport. The variations in human mobility over this period of time were calculated for the United States, United Kingdom, Italy and Germany using 13 January as the baseline. A clear drop in the 4 curves is seen when the WHO officially declared a global pandemic (11 March 2020). In Italy, one of the countries that was the most affected, human mobility decreased more than 80% in April compared to the beginning of the year 2020. Interestingly, a recovery is seen during the 2020 summer months followed by a second decline in the winter of 2020 – 2021, however less strong than the first one. Indeed, the situation was more stable last summer resulting in more flexible covid-19 measures whereas at the end of 2020 a second lockdown was announced. This data strongly suggests that strict covid-19 measures resulting in limited outdoor activities reduced human's mobility worldwide.

All these different indicators could be implemented to get a better idea of how the lockdown period can be defined. Moreover, they can be used to demarcate specific periods of reduced human activity. Out of the data described in this section, it is safe to say that the lockdown in 2020 was the most pronounced between mid-March and June. This suggests that the largest effect for the air pollutants included in this study might be expected within this period.

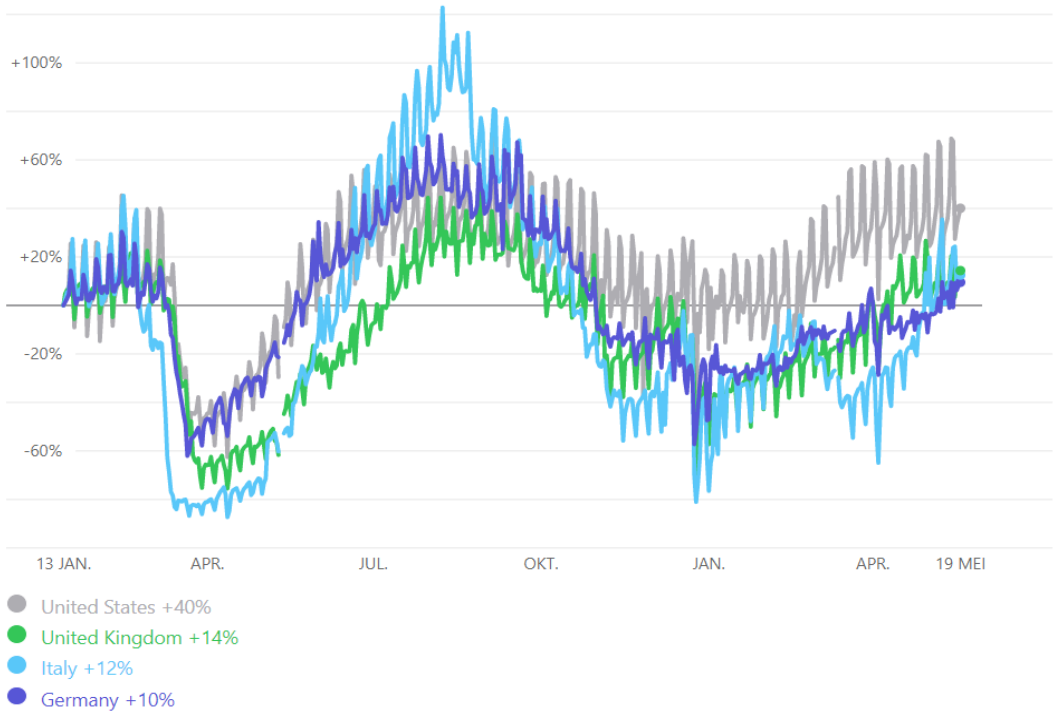

Figure 4.1. Human mobility in terms of driving and the use of public transport for 4 different countries across the world, with 13 January 2020 as the baseline (Apple mobility report).

4.2. Comparison between the reference multiyear time series and 2020 abundances of the individual air pollutants

4.2.1. Data processing

The multiyear time series that were obtained for each included air pollutant were compared to their 2020 abundances, expressed in monthly means. The 2020 FTIR spectra of the species were filtered and processed in the same way as the multiyear time series were handled (see chapter 3). However, as the data for 2020 only includes one year of measurements there was no trend analysis and detrending of the time series performed. Monthly means of 2020 for the different air pollutants were calculated and used to directly compare to the multiyear time series, also expressed in monthly means. Important to note is that a specific device of the FTIR spectrometer at Jungfraujoch broke up in August 2020 and second part of December 2020. For this reason, there will not be any data displayed on the plots corresponding to these periods (a gap for August 2020 will be seen).

Due to time limitations to further carry out this work, no statistical analyses were performed on the outcomes of the multiyear comparison with the 2020 time series. The data was visually compared and interpreted.

4.2.2. Acetylene

Figure 4.2. shows the comparison of the different time series for acetylene (C_2H_2), expressed in monthly means. The orange line illustrates the monthly mean total columns for year 2020. The blue lines represent the years 2010 to 2019 where the lightest tint of blue corresponds to 2010 which darkens if we progress in time. The average monthly means for this 10-year period are shown in black together with the +- 1σ standard deviation (vertical bars). All other individual species described in the next sections are presented in the exact same way.

For C_2H_2, the largest difference between the multiyear time series and 2020 was seen for the months January and February where lower values were observed in 2020 (Figure 4.2.). From March, when the lockdown started, to June the 2020 curve seemed to approach the multiyear average curve. This exact period (March – June) was characterised by a 6.81% concentration decrease in 2020 compared to the last decade. No specific conclusions could be drawn for the second half of the year 2020. The most pronounced peak in the multiyear time series probably corresponded to the 2018 California wildfire season releasing large amounts of C_2H_2 and other VOCs into the air. This was one of the deadliest and most destructive fires of all times

(https://www.fire.ca.gov/stats-events/). For C_2H_2, no clear conclusions on the effect of the lockdown could be made only based on this figure. However, in the first half of the year 2020, the average C_2H_2 concentrations were found below the average of the past decade. Statistical and back-trajectory analyses will be needed to further clarify these results.

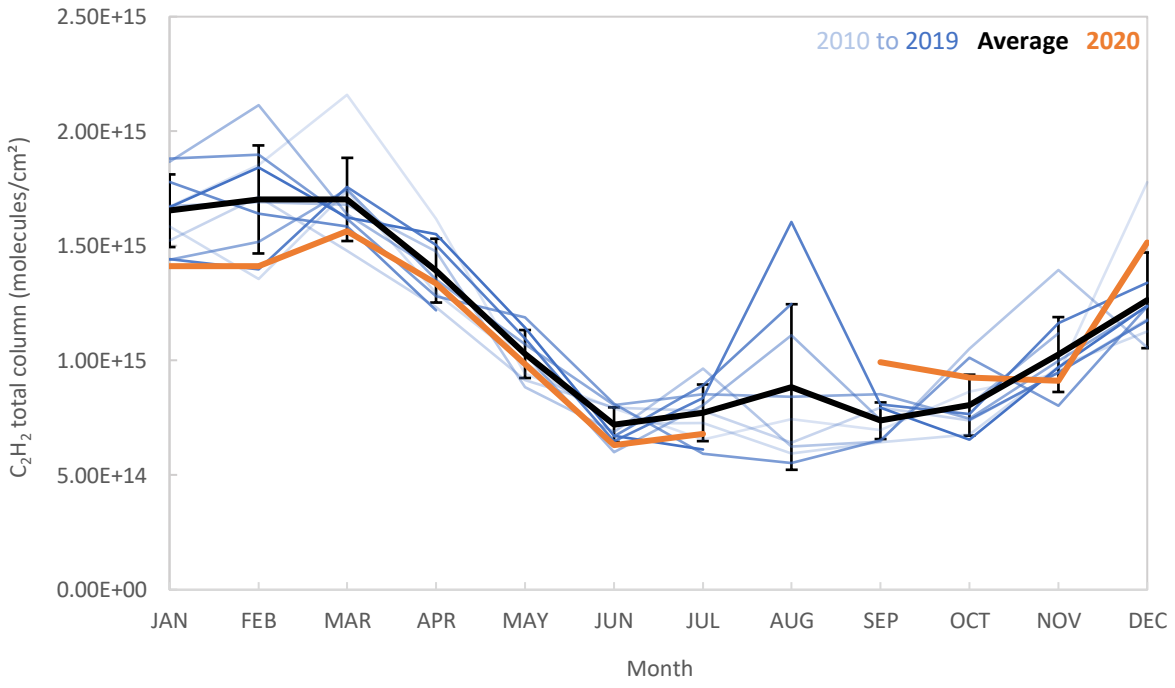

Figure 4.2. Acetylene (C_2H_2) monthly means at the Jungfraujoch. The orange line shows the year 2020. The blue lines indicate the year 2010 to 2019 with their average and 1 sigma standard deviation in black.

4.2.3. Ethylene

Next to C_2H_2, ethylene (C_2H_4) is also a VOC for which biomass burning is a dominant source. Beside some abnormalities, the comparison between the year 2020 and the 10-year time series looked more or less similar for C_2H_4 and C_2H_2 (Figure 4.3.). The 2020 mean total columns were visually lower compared to the past decade from January until May where the first two months had the most pronounced difference. Next to biomass burning, C_2H_4 can also be produced through industrial processes to make for example plastics. As most parts of the industry sector were put on hold during the first lockdown, or were less active, it is not very surprising to see some minor decreases in C_2H_4 concentrations from mid-March to May. However, a statistical analysis of the related values is needed before drawing firmer conclusions.

An unexpected average increase during the lockdown period (March – June; as discussed in section 4.1.) in 2020 compared to 2010 - 2019 of was seen for this air pollutant. A large peak was observed in June 2020. There is currently no explanation for this and also no objective reason was found to reject any values for that month. Another peculiarity that has revealed itself is the extremely high monthly mean for August (about 10 times higher than the other means) corresponding to the year 2017. This had to do with a fire plume was passing over the Swiss Observatory site coming from a large wildfire in the Canadian forests in British Columbia (https://www2.gov.bc.ca/gov/content/safety/wildfire-status). Although the lifetime of C_2H_4 is only a few days, we can still see a strong signature of the wildfire which means that the measurements are quite sensitive. However, these extreme high concentrations make it less feasible to draw interesting conclusions regarding covid-19 and thus should be accounted for. The California wildfires of August 2018 are also projected in this figure, although less pronounced. December 2020 also shows high abundances which cannot be explained for the moment. It might perhaps be related to a sink effect as there is a minimum concentration of OH available during that time of the year. This monthly mean corresponds to only 3 measurements by the FTIR spectrometer as the instrument was not operating most of the time during that month.

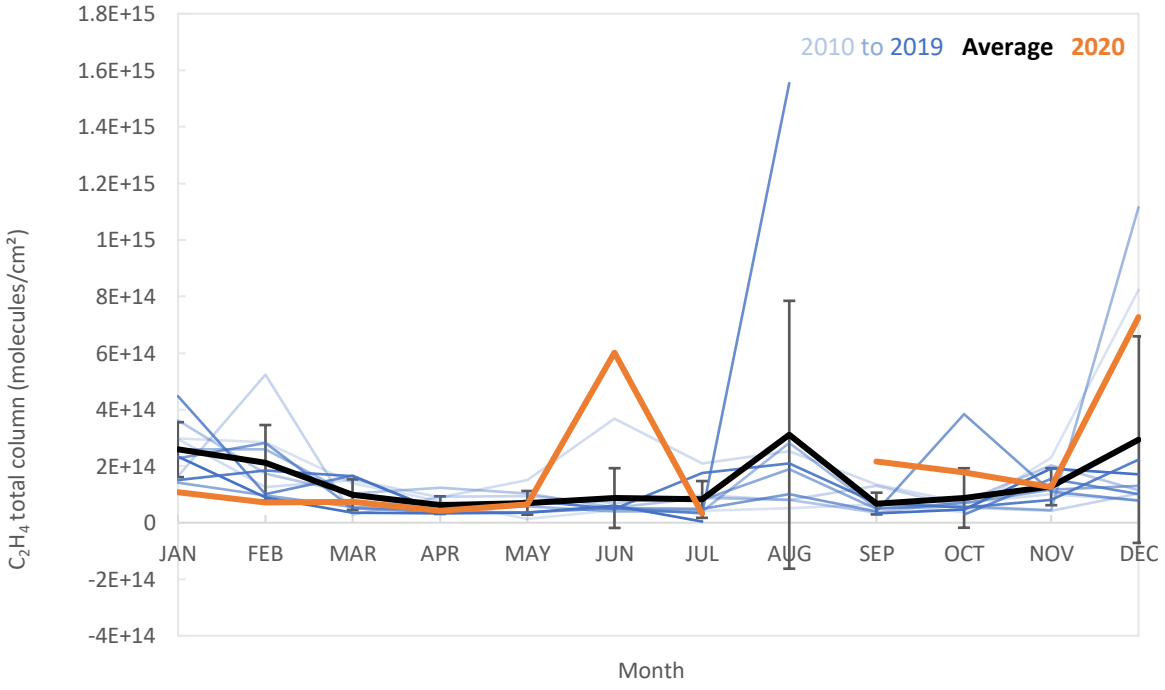

Figure 4.3. Ethylene (C_2H_4) monthly means at the Jungfraujoch. The orange line shows the year 2020. The blue lines indicate the year 2010 to 2019 with their average and 1 sigma standard deviation in black.

4.2.4. Ethane

The curves of C_2H_2, C_2H_4 and ethane (C_2H_6) all seem to have a similar shape, including the 2020 data. Figure 4.4 shows the C_2H_6 total columns where the 2020 concentrations were again on a low during the first months of the year compared to the last decade. The lockdown period (March – June 2020) indicated an average decrease of 3.55% compared to the 10-year time series of the same months. In contrast to the other gases (C_2H_2 and C_2H_4) the 2020 lines stayed most of the time below the 10-year average. C_2H_6 is mostly an indicator of the oil and gas sector with shale gas exploitation being a significant contributor to its emissions. Fluctuations of the oil price on the market have significant interannual consequences on the exploitation of the wells (low prices means non-profitable activity). This possibly explains the drop in C_2H_6. This is in line with a study of Deloitte who has reported a 30% decrease in the demand for petroleum in April (Deloitte, 2020). Biomass burning is only accounting for 18% of the ethane emissions (Xiao et al., 2008).

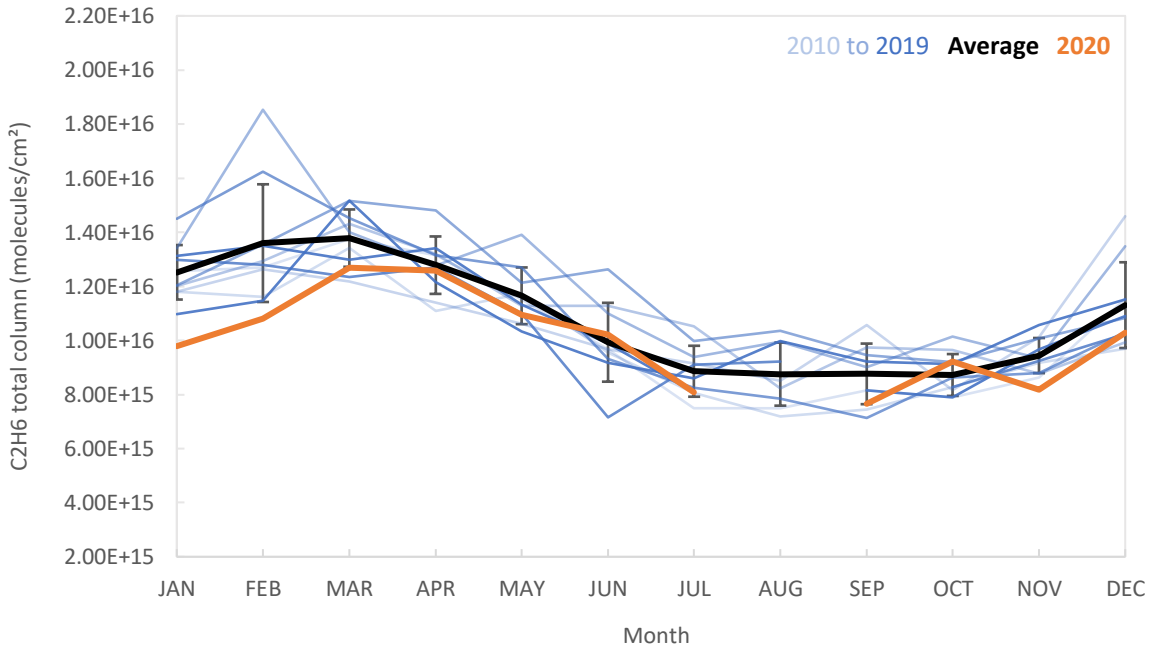

Figure 4.4. Ethane (C_2H_6) monthly means at the Jungfraujoch. The orange line shows the year 2020. The blue lines indicate the year 2010 to 2019 with their average and 1 sigma standard deviation in black.

4.2.5. Methane

As the second most abundant anthropogenic greenhouse gas and important precursor of ozone, methane (CH_4), is an interesting species to observe. Figure 4.5. reveals that the year 2020 was not characterised by lower CH_4 concentrations, on the contrary, concentrations were higher during lockdown than the past 10-year average (average increase of 1.01% from March to June 2020). Although CH_4 has large anthropogenic sources, such as domestic ruminant animals and rice cultivation, the production of these sources was barely decreased during lockdown period as these contain the production of human basic needs (Kirschke et al., 2013). Moreover, wetlands also significantly contribute to its emission which were, as a large biogenic source, not affected by a drop in human activity. These results suggest that the CH_4 abundances were not affected by the covid-19 related lockdown.

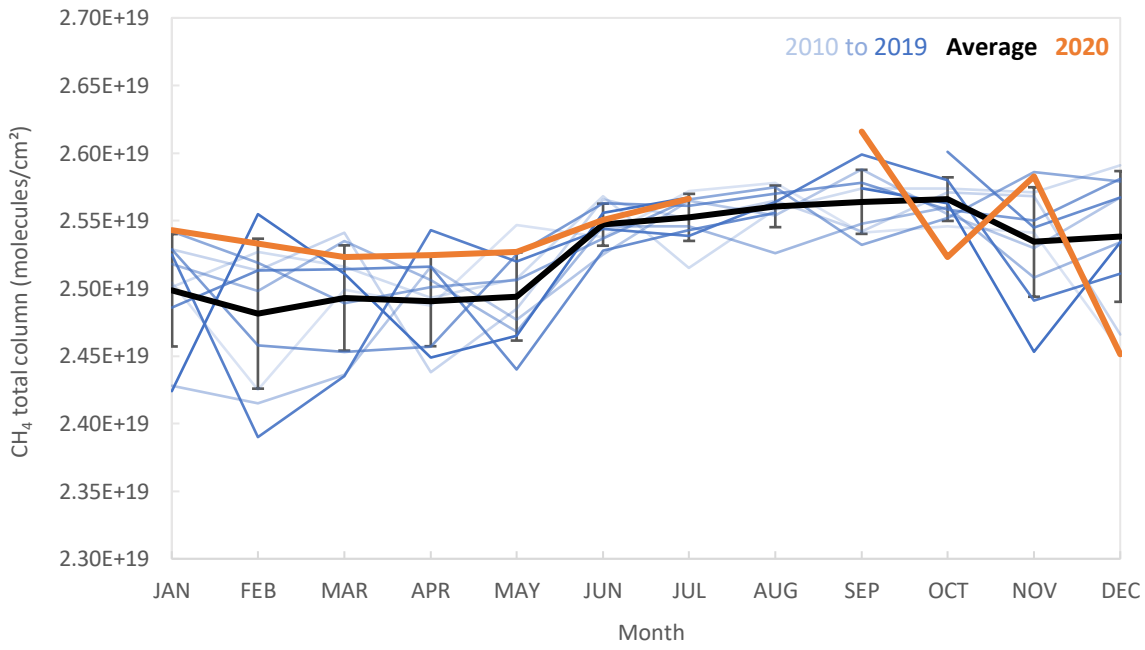

Figure 4.5. Methane (CH_4) monthly means at the Jungfraujoch. The orange line shows the year 2020. The blue lines indicate the year 2010 to 2019 with their average and 1 sigma standard deviation in black.

4.2.6. Methanol

Methanol (CH_3OH) has mainly biogenic sources (plant growth) so it was indeed expected not to see a lot of differences in 2020 in comparison to the last decade (Figure 4.6.). From March to June 2020, an average decrease of 0.58% was found. Interesting, the April 2020 monthly mean is the lowest measured value of the past decade. Fossil fuel combustion, industrial activity and vehicular emission are some minor anthropogenic sources of CH_3OH that could provide a possible explanation for low April values in 2020 (the lockdown was the strictest in April). However, this is not compliant with other gases also being produced out of these typical sources (e.g. C_2H_2 and CO) that do not have the same response in April. Further research will be needed to clarify this peculiarity and define if CH_3OH was affected by the lockdown in April.

It is worth to mention that 2 peaks can be seen for 2018, namely in May and August. For May 2018, it was found that there was only one measurement retrieved during that month that happened to be an elevated value (± 2 times higher than the 10-year mean). Therefore, no clear conclusions can be drawn from this peak. The second peak in August is likely due to the 2018 California wildfires as seen for some other VOCs since the total columns of the entire month were on a rise (Yokelson, 1999).

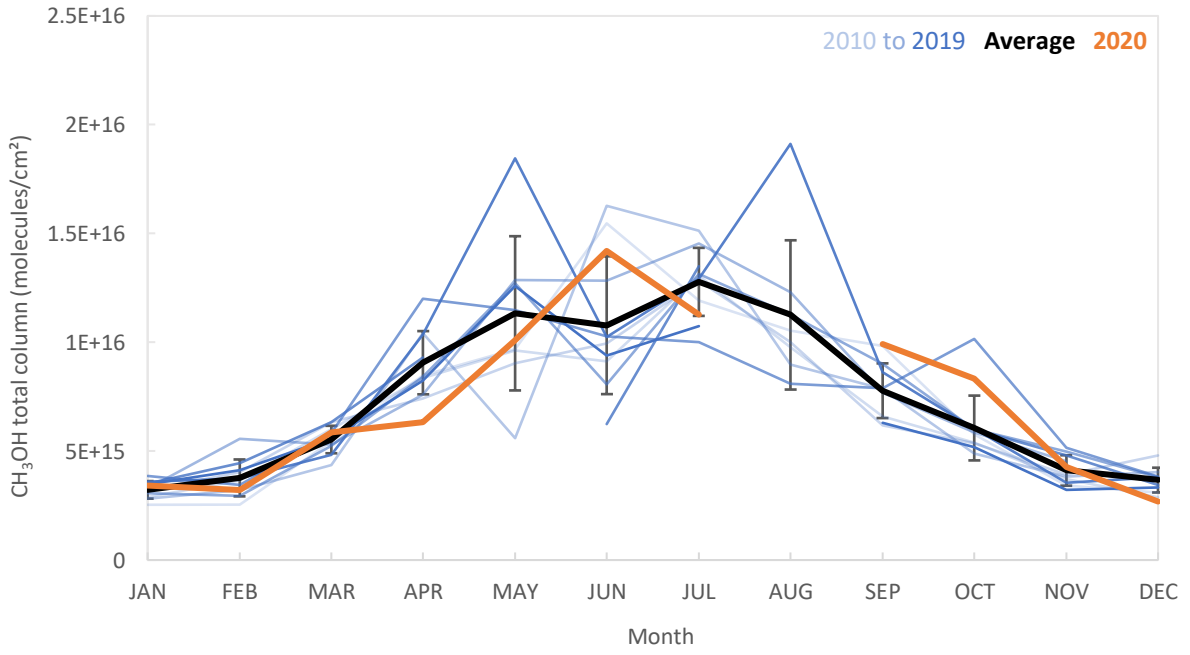

Figure 4.6. Methanol (CH_3OH) monthly means at the Jungfraujoch. The orange line shows the year 2020. The blue lines indicate the year 2010 to 2019 with their average and 1 sigma standard deviation in black.

4.2.7. Formaldehyde

Figure 4.7. represents the formaldehyde (H_2CO) monthly means which clearly indicate that the mean 2020 values from April to July were lower than the 10-year averages. In this study, the calculated decrease in the average H_2CO concentrations during lockdown (March – June 2020) corresponded to -13.65%. Another study already found significant decreases (-11%) in 2020 compared to 2019 in China which could partially be explained by the lockdown (Sun et al., 2021). Since H_2CO is largely produced from non-methane VOC (NMVOC) oxidation in the troposphere a decrease in its concentration during lockdown was indeed expected. Further research must find out to what extent this relatively low H_2CO abundance from April to July 2020 can be attributed to the covid-19 lockdown. Here again, the peak in August 2018 showed itself probably representing the California wildfires (Yokelson, 1999).

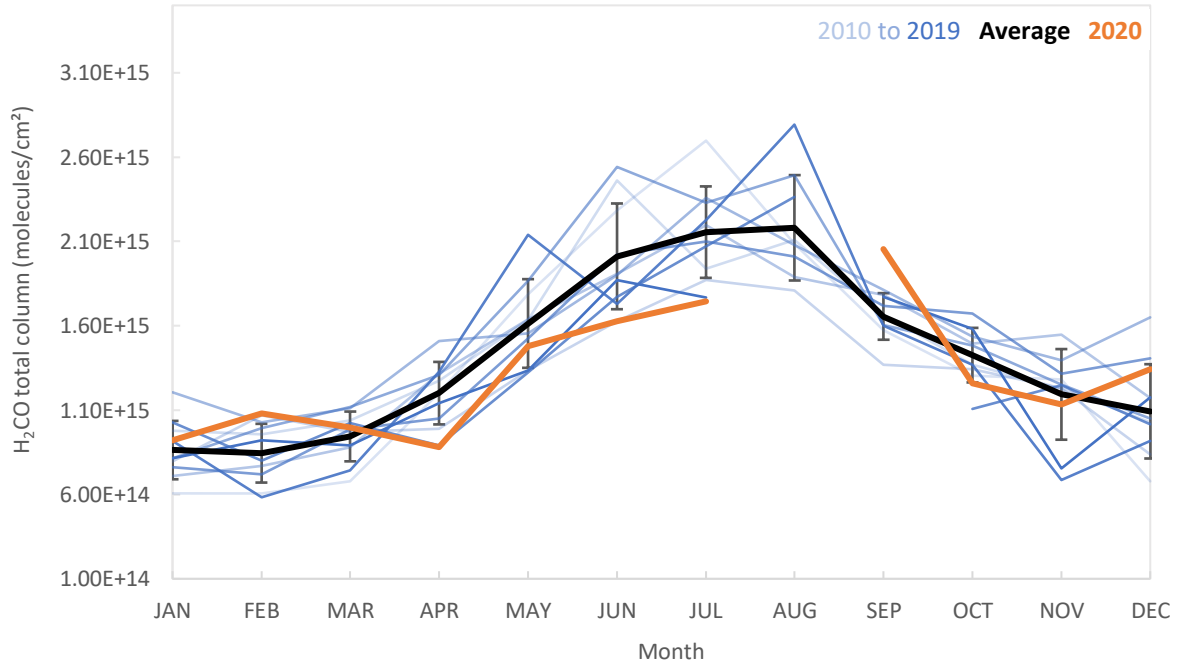

Figure 4.7. Formaldehyde (H_2CO) monthly means at the Jungfraujoch. The orange line shows the year 2020. The blue lines indicate the year 2010 to 2019 with their average and 1 sigma standard deviation in black.

4.2.8. Hydrogen cyanide

The hydrogen cyanide (HCN) 2020 curve of Figure 4.8. does not show any special features in comparison to the 10-year time series average. Average concentrations increased with 6.50% from March to June 2020 in comparison with the 10-year average. This could be attributed to the biogenic sources of HCN that are dominant in its production and are thus poorly affected by decreased human activity.

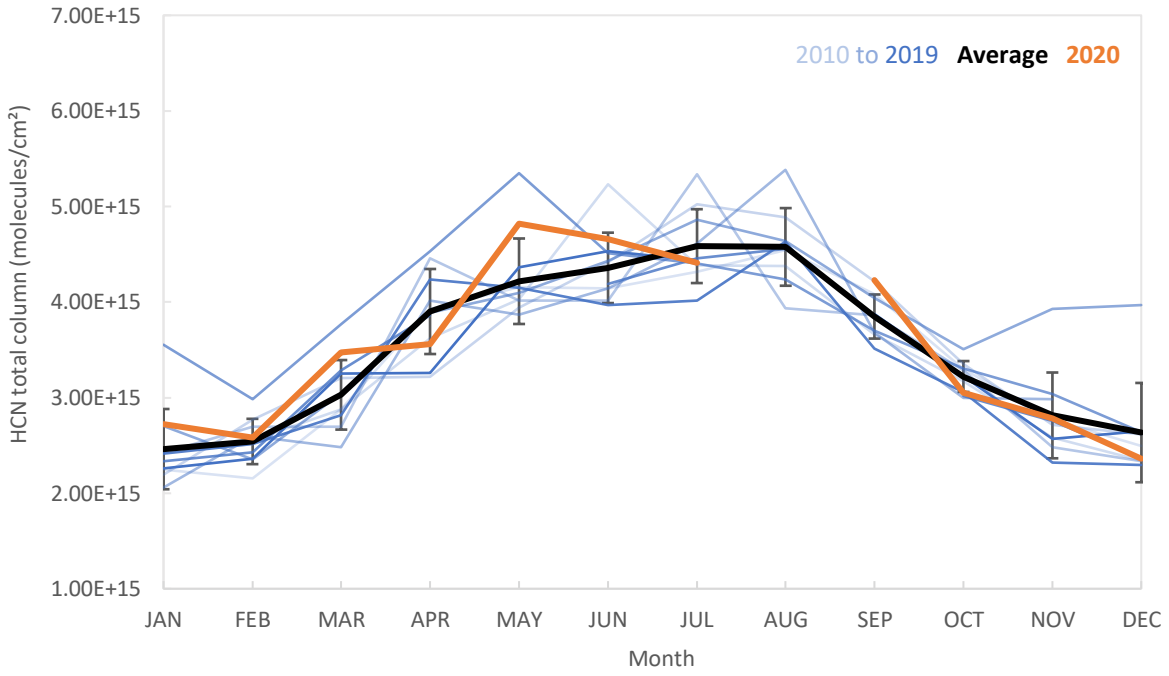

Figure 4.8. Hydrogen cyanide (HCN) monthly means at the Jungfraujoch. The orange line shows the year 2020. The blue lines indicate the year 2010 to 2019 with their average and 1 sigma standard deviation in black.

4.2.9. Formic acid

In figure 2.9., formic acid (HCOOH) was characterised by decreased mean total columns in the first five months of 2020 compared to the 10-year time series. April and May 2020 even showed the lowest abundances over the past decade. The lockdown period showed a decrease of -9.09% in comparison to the last decade. HCOOH can be produced from CH_3OH in industrial processes, and indeed, similar behaviour of both curves in the March and April 2020 was seen (Figure 4.6.). HCOOH is commonly used in the leather and textile industry. As those industries were put on hold in March 2020, the drop in the HCOOH 2020 curve could be related to the start of the lockdown. However, more research will be needed in order to confirm or further specify this.

Again, the peak concentration in August 2018 could be attributed to the California wildfires as HCOOH is largely emitted by wildfires. Another peak is seen for the June 2020 monthly mean. As discussed in section 4.2.3., C_2H_4 had a similar feature at the same time and period. However, when looking in more detail to the data of both species, there could no direct connection be made between those peaks. In contrast to C_2H_4, which only shows elevated concentrations for the 1st of June 2020, HCOOH total columns is increased for the whole month of June. No explanation for this can be given at the moment.

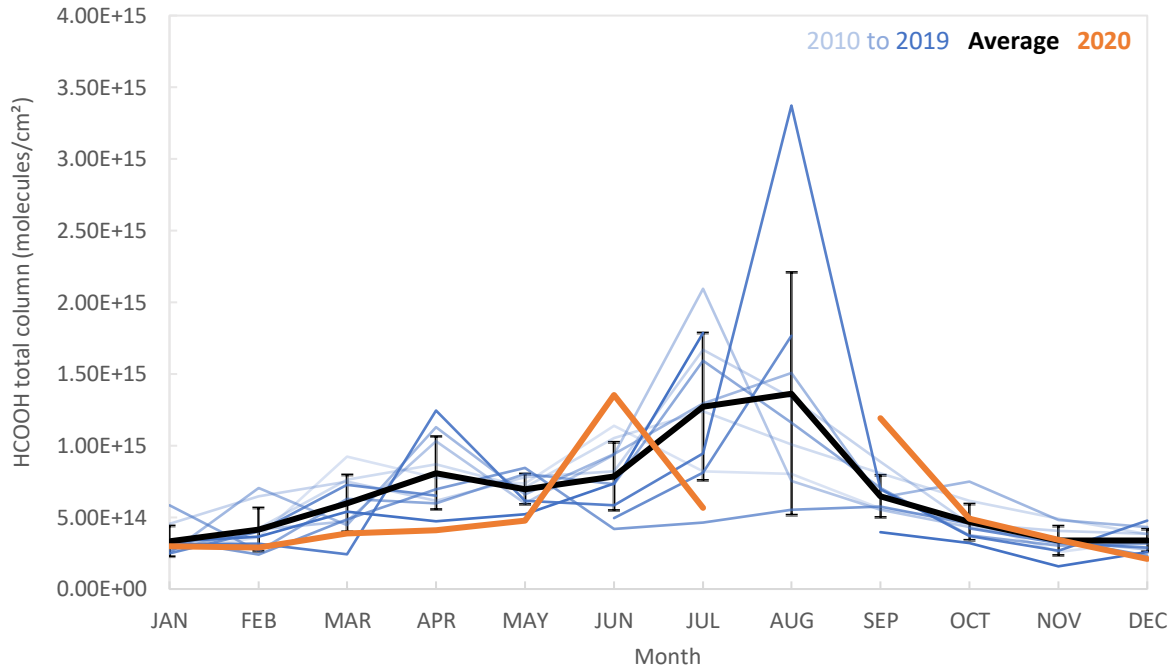

Figure 4.9. Formic acid (HCOOH) monthly means at the Jungfraujoch. The orange line shows the year 2020. The blue lines indicate the year 2010 to 2019 with their average and 1 sigma standard deviation in black.

4.2.10. Carbon monoxide

Although carbon monoxide (CO) is mainly produced by anthropogenic sources, Figure 4.10. shows no special behaviour of the CO 2020 curve during the lockdown period. In fact, a small increase of 3.07% was observed from March to June 2020. CO emissions largely result from thermal combustion which probably did not decrease much as houses still needed to be warmed during the first months of lockdown. Also, reductions in CO due to decreased road traffic are mostly not reflected in the free troposphere above Jungfraujoch, only when ABL air is more sampled at the site because of the unusual meteorology. However, it must be noted that there are other studies showing a significant decrease in CO concentrations during

lockdown. For example, Kerimray et al. found a reduction in CO concentrations of 49% compared to the 17 days prior to lockdown in Almaty, Kazakhstan (Kerimray et al., 2020). Two other studies also reported decreased CO emissions worldwide in March and April 2020 (Mahato et al., 2020; Sannigrahi et al., 2021). The contradictory result of this study may indicate that nontraffic related CO sources were possibly more at play at Jungfraujoch site of observation.

As CO can also be emitted by fires, the highest peak in August 2018 provides another evidence of the extent and spread of the Californian wildfires.

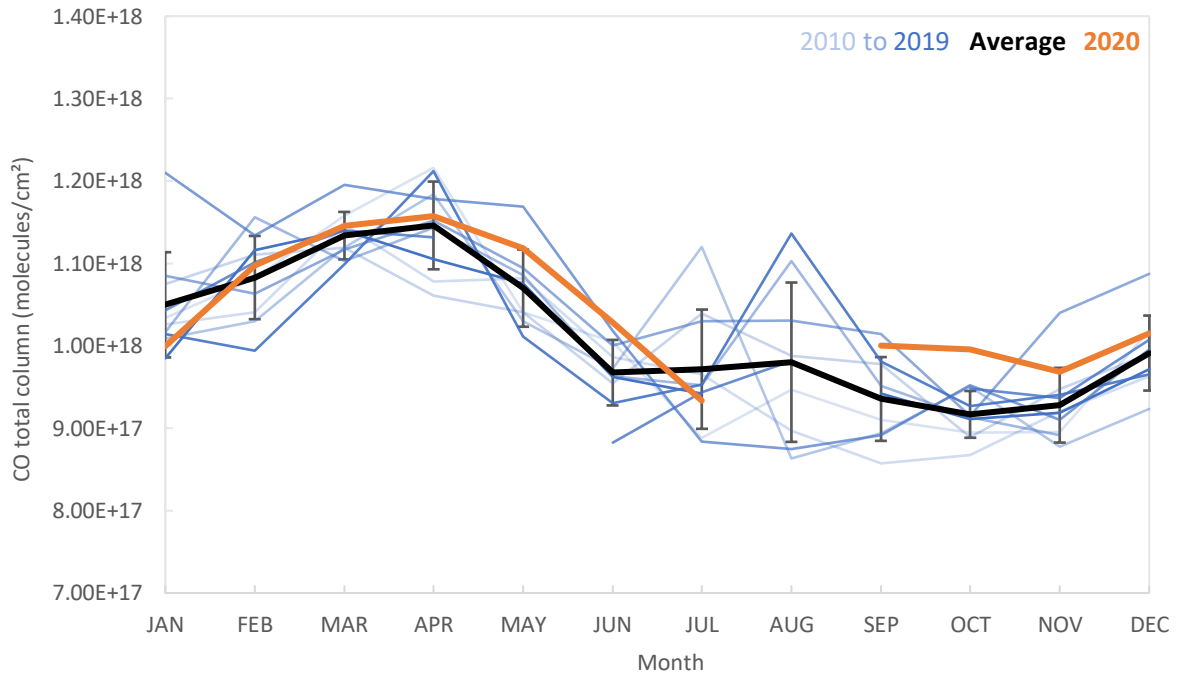

Figure 4.10. Carbon monoxide (CO) monthly means at the Jungfraujoch. The orange line shows the year 2020. The blue lines indicate the year 2010 to 2019 with their average and 1 sigma standard deviation in black.

4.2.11. Ammonia

Ammonia (NH_3) abundances are presented in Figure 4.11. The NH_3 abundances of the year 2020 were rather unambiguous and did not show any clear decrease in comparison to the multiyear time series. In fact, an average increase of 17.12% from March to June 2020 was observed. Agricultural practices are an important source of this air pollutant which possibly explains the unaltered concentrations of NH_3 as a response to the lockdown. The highest monthly mean for the last 10 years has been observed for May 2020. When looking at the NH_3 2020 data, it was seen that the mean total columns were about 6 times higher on 21 May than

the average concentration for that year. This could possibly have to do with surrounding agricultural activities at the Jungfraujoch. When neighbouring farmers spread out their fertilisers and upslope winds are present, strong outliers of the NH_3 data can be generated. Also for NH_3, the effect of the wildfires in California in August 2018 was observed because biomass burning is also an important NH_3 source (Bray et al., 2018). As 2020 was also characterised by some enormous fires in that region, the peak value for September 2020 might also correspond to this.

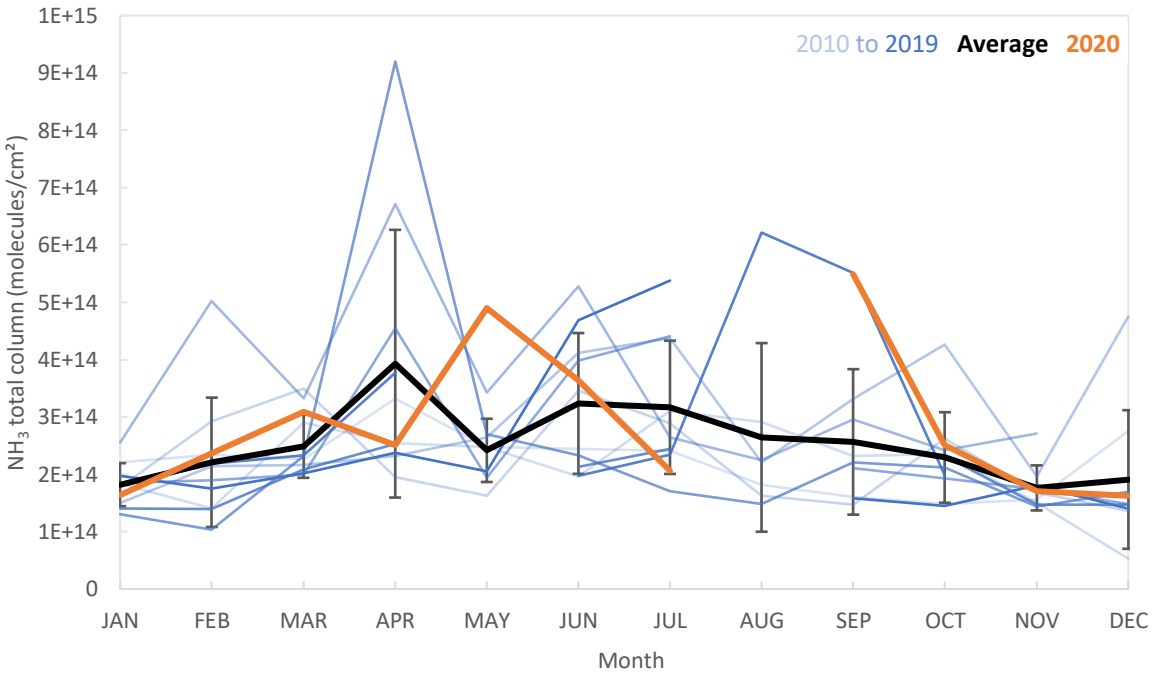

Figure 4.11. Ammonia (NH_3) monthly means at the Jungfraujoch. The orange line shows the year 2020. The blue lines indicate the year 2010 to 2019 with their average and 1 sigma standard deviation in black.

4.2.12. Tropospheric ozone

The results obtained for tropospheric ozone (O_3) are represented in Figure 4.12. Here, a 20-year times series was used (2000 – 2019) to compare the 2020 data to instead of a 10-year period as for the other studied air pollutants. Also, the volume mixing ratios at tropospheric altitude were considered by taking the mean of all the levels from the lowermost partial column to about 10 km altitude (3903 m – 10250 m). The 2020 O_3 concentrations were clearly decreased during the first half of 2020 in comparison with the multiyear time series average. Moreover, in February, April and May 2020 the lowest concentrations in O_3 were observed for the last two decades. For this study, the decrease during lockdown corresponded to -13.39%.

These observations are in line with the results of Steinbrecht et al., who also compared O_3 monthly means in 2020 to 2000 – 2019 values monitored at Jungfraujoch (only at 6 km altitude) (Steinbrecht et al., 2021). In the Steinbrecht study, a significant reduction of 7% was found in spring and summer of 2020 in the northern extratropical free troposphere (other stations were also included). Weber et al. used model simulations to look at air pollutant emission reductions in 2020 and also found similar results to Steinbrecht et al. and this study (Weber et al., 2020). Furthermore, their simulations could link the reduced emissions to road and air traffic during the period of lockdown. These results strongly suggest that reduced emissions of tropospheric ozone precursors due to the covid-19 lockdown are large enough to affect ozone abundances at Jungfraujoch. However, it is important to note that unusual meteorological conditions in 2020 could also affect the O_3 concentrations. It was for example seen that the Arctic ozone depletion reached a record level during the winter of 2019 – 2020 (World Meteorological Organization (WMO), 2020).

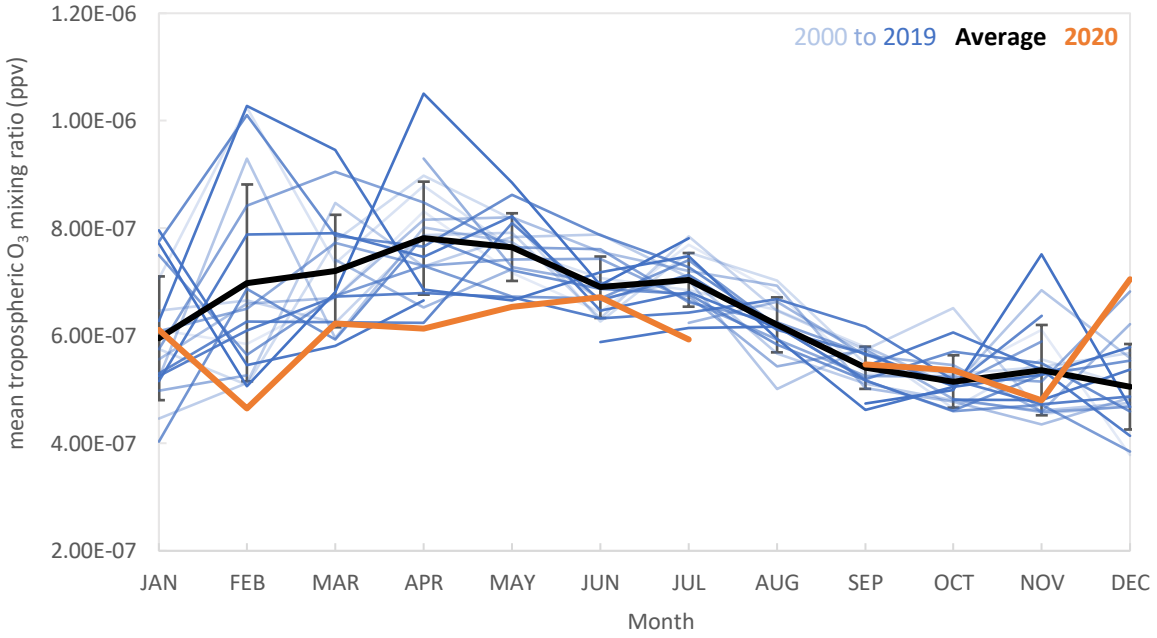

Figure 4.12. Ozone (O_3) monthly means at the Jungfraujoch. The orange line shows the year 2020. The blue lines indicate the year 2000 to 2019 with their average and 1 sigma standard deviation in black.

4.3. The average change in tropospheric ozone precursors during lockdown

4.3.1. The VOCs

The visual interpretations of the individual studied air pollutants showed that most VOCs have decreased abundances in the first half of the year 2020 compared to the 2010 - 2019 monthly averages. Only for HCN, this was not the case. As explained in section 1.2.3. VOCs are important in the production of tropospheric O_3. By making an average of all the VOCs monthly means that were included in this study, a better understanding in the reduced tropospheric O_3 concentrations during lockdown could be achieved. Figure 4.13. illustrates the average monthly means of the studied VOCs (C_2H_2, C_2H_4, C_2H_6, CH_3OH, H_2CO, HCN and HCOOH) in 2020 (orange line) and 2010 – 2019 (black line) and the corresponding variation in O_3 concentration for each month. In order to generate the upper panel of this figure, daily means for each species were calculated only including the days on which data for all the gases was retrieved. This way, monthly means could be calculated for each year. The lower panel represents the ratio between the 2020 and 2000 – 2019 monthly means of O_3 (for each month separately), expressed in %.

In Figure 4.13, decreased abundances of the VOCs can be observed for the first half of year 2020 in comparison to the last decade. For February and March, the 2020 monthly means lie within the 1 sigma standard deviation (StDev) of the 10-year average. However, for April and May, the 2020 VOC concentrations were clearly lower than the last decade corresponding to a reduction of -14.7% and -13.9%, respectively, where April even reached the lowest value in a decade. No specific conclusions can be drawn for the second part of the year 2020 (from June to December). Here, the VOCs seemed to be restored and even reached the highest abundance in September since the last decade. These changes in VOC concentrations are translated in the tropospheric O_3 variations in the year 2020 (blue curve). The variations in tropospheric O_3 concentrations correspond to a reduction of -21.5% and -14.5% for April and May, respectively (2020 compared to the average of 2000-2019). Out of the visual interpretation of the plots, we can state that a reduction of the total VOCs during the first half of 2020 was, at least partly, related to the declined tropospheric O_3 concentrations at the same period. It is strongly believed that the covid-19 lockdown was a cause of this decrease. However, further research is needed in order to consolidate this statement and define to what extent the lockdown contributed to the drops in total columns of these air pollutants, in particular with the support of dedicated model simulations implementing business as usual versus lock-down representative emissions.

Next to VOCs, NO_x are also major tropospheric O_3 precursors. We don't have the information on the NO_x abundances at Jungfraujoch because the site is not polluted enough to actually monitor it. Other studies agree that also NO_x concentrations were reduced during the lockdown period, worldwide. Guevara et al. for example found a decrease of -33% in NO_x from March to April 2020 in Europe, whereas Venter et al. reported a -29% global decline in NO_2 (Guevara et al., 2021; Mahato et al., 2020; Venter et al., 2020). As explained in section 1.2.3., the VOC/NO_x ratios can influence the O_3-NO_x-VOC chemistry and so the production of tropospheric O_3. Kermiray et al. showed that in highly polluted cities (low VOC/NO_x ratio), O_3 concentrations indeed increased (+15%) during lockdown because of the significant decrease in NO_x (Kerimray et al., 2020). Similar results were also reported by other studies which confirm the effect of decreased human activity on air pollutants (Collivignarelli et al., 2020; Siciliano et al., 2020).

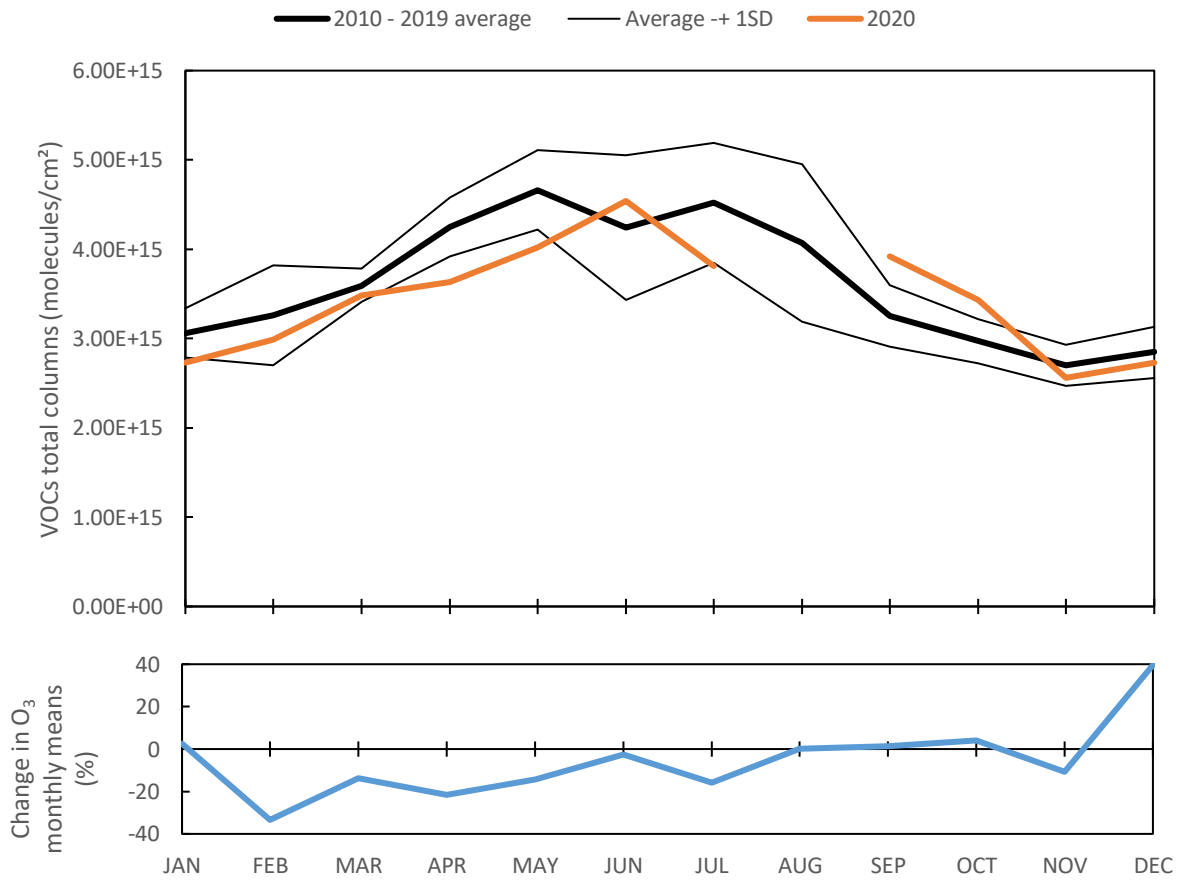

Figure 4.13. Observed monthly means of all the included VOCs at Jungfraujoch and corresponding variation in O_3 concentration (in %) for each month. Monthly means for 2020 are given in orange, the average of the 2010 – 1019 monthly means are shown in black together with their +- 1σ standard deviation. The blue line in the lower panel represents the increase/decrease in O_3 monthly mean concentrations in 2020 compared to the reference multiyear average (2000 – 2019).

4.3.2. Carbon monoxide and methane

Next to VOCs and NO_x, CO and CH_4 are also amongst the most important precursors of tropospheric O_3. In this study, no decrease in concentrations of both air pollutants could be observed (see section 4.2.5. for CH_4 and section 4.2.10. for CO). For CH_4, monthly means even seemed to be on a high during the first part of 2020. The poor changes in CO concentrations during lockdown was confirmed by the results of a study of Sannigrahi et al. only showing some minor decrease from February to May 2020 for 20 cities across the world compared to the same period in 2019 (Sannigrahi et al., 2021). The elevated concentrations in CH_4 are also reported by the company Kayrros (https://www.kayrros.com/) which is a global leader in climate data analysis. A study conducted by this company found through satellite measurements an increase in CH_4 emissions of 32% during the first 8 months of the year 2020 compared to the same period in 2019. This was mainly attributed to the methane plumes emitted from Russian gas infrastructure (Beitsch, 2020). These findings may suggest that CO and CH_4 did not stimulate the decrease in tropospheric O_3 formation during lockdown. More research is needed to further disentangle these results.

4.4. Future research perspectives

Although we have kept it simple because of time constraints, interesting visible differences in tropospheric air pollutant concentrations during lockdown have been found. These results are of importance since this is the first time that most of these pollutants' abundances at Jungfraujoch were studied in the context of the covid-19 pandemic and lockdown.

Further analysis of the results will be needed in order to indicate if these drops in concentrations are statistically significant and to what extent the lockdown has played a role in the reduced air pollutant concentrations. Many factors, including meteorological conditions, the strictness of the lockdown measures and other sources of variations in emissions are also influencing the abundance of the air pollutants and thus need to be identified. Meteorological conditions, such as for example the humidity, temperature, precipitation and wind speed and direction can affect the local atmospheric air pollutant amounts (Goldberg et al., 2020; Ordóñez et al., 2020). More specifically, some of these conditions could favor upslope winds, bringing polluted ABL air from the valleys on top of the mountains. In addition, large wildfires are known to strongly alter the emissions of specific tropospheric gases, as shown in this study.

Since June 2008, ^{222}Radon (^{222}Rd) data are publicly available for the Jungfraujoch station from the University of Basel (https://azug.minpet.unibas.ch//~lukas/pl/radon.pl). This dataset allows to identify episodes of anabatic or upslope winds bringing air from the surrounding valleys to

the mountaintop. As the Jungfraujoch Observatory is mainly located in the free troposphere (clean air), ABL polluted air can be detected this way and taken into account when monitoring the different air pollutant concentrations. ^{222}Rd data is thus important to determine whether the measurements have been affected by the ABL air instead of free tropospheric air. This could clarify to what extent the reduced air pollutant concentrations during lockdown 2020 can be explained by the meteorological conditions, and to which extent, or by a real drop in emission. As the ^{222}Rd data could be a promising source of information it is suggested to be investigated in the future.

For the complete interpretation and quantification of the results, model simulation data will be needed. Modelling studies can help getting a better insight in what the exact causes for the decreased and sometimes increased emissions or abundances are. Different sectors and industries, such as for example road and air traffic, can be studied this way and reveal their exact contribution to the variations in air pollutants emission (Weber et al., 2020).

5. Conclusions

This study evaluated the effects of the covid-19 pandemic lockdown on the abundance of different tropospheric air pollutants monitored at Jungfraujoch. Focus was put on carbonaceous ozone precursors and ozone itself. In general, a decrease in their concentration was observed during the first half of the year 2020, especially for the months March, April and May.

A first challenge of this work was to construct reference multiyear time series of the included gases that could be used for comparison with the measured abundances of year 2020. Vertical profiles and total columns retrieved from FTIR spectra recorded at the Jungfraujoch Observatory were processed to compute monthly means for each individual species over a certain period of time. Due to limitations to extensively perform this research, a 10-year period (2010 – 2019) was chosen as the reference to compare the 2020 data to, except for O_3 (20 years). Importantly, we still must ask ourselves what the minimum extension of the climatological time series should be to build a representative dataset. If there was more than three months of time to perform this study, we would be able to answer this question and examine if ten years for the reference period would suffice. However, some interesting findings were obtained using the data from the past decade. The trend of the monthly means for each species was analysed using the bootstrap resampling method where they were detrended if needed. A statistically significant trend from 2010 to 2019 was found for the next air pollutants: C_2H_2, HCN, CO (decreasing trend) and C_2H_6, CH_4, H_2CO and NH_3 (increasing trend).

A second challenge of this work was to compare the 2020 monthly means of the included air pollutants to the reference multiyear time series. Visual interpretation of the data showed that for C_2H_2, C_2H_4 and C_2H_6, the decreased abundance was the most pronounced at the beginning of the year 2020, before the emergence of the virus was officially declared as a pandemic. Covid-19 was for the first time detected in December 2019 in Wuhan and on 23 January 2020 the Chinese city together with some neighbours were quarantined. However, on a large scale, no strict lockdown measures were taken in China during that period, even not in February 2020. Therefore, we cannot state that the reduced abundances of these species have a connection with the covid-19 lockdown. Further research is needed to clarify this specific drop in concentrations during the first 2 or 3 months of the year 2020. The other studied NMVOCs (CH_3OH, H_2CO and HCOOH) showed a clear drop in concentration during the lockdown period, especially from March to May. As a consequence of the reduced NMVOC concentrations during the first part of the year 2020, lower tropospheric ozone abundances were also found above Jungfraujoch at that period. For CH_4, CO, HCN and NH_3, we found no

concluding or robust evidences of an effect of lockdown on their abundances. Here again, more time would be required in order to further analyse and interpret the results. We now limited ourselves to the visual interpretation of the data, however statistical analysis is needed to deliver robust conclusions. Also, additional studies including model data, will be needed to show the potential correlation between decreased human activity during lockdown and lower NMVOCs and ozone abundances. Beside all this, it is important to note that this data was looked at for the first time in this specific research context, providing a basis for future research.

We can conclude that most of the studied tropospheric air pollutants above Jungfraujoch showed reduced abundances during the 2020 lockdown, and the largest effects were seen for the VOCs and tropospheric O_3. However, caution is needed for the interpretation of these results. Further research must clarify and quantify the exact impact of the covid-19 lockdown upon European air pollutant emissions.

6. References

Al-Saeed, T., & Khalil, D. (2010). Diffraction effects in optical microelectromechanical system Michelson interferometers. *Appl. Opt.*, *49*, 3960–3966.

Bader, W., Bovy, B., Conway, S., Strong, K., Smale, D., Turner, A. J., Blumenstock, T., Boone, C., Collaud Coen, M., Coulon, A., Garcia, O., Griffith, D. W. T., Hase, F., Hausmann, P., Jones, N., Krummel, P., Murata, I., Morino, I., Nakajima, H., … Mahieu, E. (2017). The recent increase of atmospheric methane from 10 years of ground-based NDACC FTIR observations since 2005. *Atmospheric Chemistry and Physics*, *17*(3), 2255–2277. https://doi.org/10.5194/acp-17-2255-2017

Bauwens, M., Compernolle, S., Stavrakou, T., Müller, J. F., van Gent, J., Eskes, H., Levelt, P. F., van der A, R., Veefkind, J. P., Vlietinck, J., Yu, H., & Zehner, C. (2020). Impact of Coronavirus Outbreak on NO2 Pollution Assessed Using TROPOMI and OMI Observations. *Geophysical Research Letters*, *47*(11), 1–9. https://doi.org/10.1029/2020GL087978

Beitsch, R. (2020). *Methane emissions up in 2020 amid turbulent year for oil and gas*. Kayrros Newsroom. https://thehill.com/policy/energy-environment/521205-methane-emissions-jump-so-far-in-2020-amid-turbulent-year-for-oil

Blumenstock, T., Hase, F., Keens, A., Czurlok, D., Colebatch, O., Garcia, O., Griffith, D. W. T., Grutter, M., Hannigan, J. W., Heikkinen, P., Jeseck, P., Jones, N., Kivi, R., Lutsch, E., Makarova, M., Imhasin, H. K., Mellqvist, J., Morino, I., Nagahama, T., … Velazco, V. A. (2021). Characterization and potential for reducing optical resonances in Fourier transform infrared spectrometers of the Network for the Detection of Atmospheric Composition Change (NDACC). *Atmospheric Measurement Techniques*, *14*(2), 1239–1252. https://doi.org/10.5194/amt-14-1239-2021

Bozem, H., Butler, T. M., Lawrence, M. G., Harder, H., Martinez, M., Kubistin, D., Lelieveld, J., & Fischer, H. (2017). Chemical processes related to net ozone tendencies in the free troposphere. *Atmospheric Chemistry and Physics*, *17*(17), 10565–10582. https://doi.org/10.5194/acp-17-10565-2017

Brasseur, G. P., & Jacob, D. (2017). Model Equations and Numerical Approaches. In *Modeling of Atmospheric Chemistry* (pp. 84–204). Cambridge University Press.

Bray, C. D., Battye, W., Aneja, V. P., Tong, D. Q., Lee, P., & Tang, Y. (2018). Ammonia emissions from biomass burning in the continental United States. *Atmospheric*

Environment, *187*(December 2017), 50–61. https://doi.org/10.1016/j.atmosenv.2018.05.052

Brown, T. P., Rushton, L., Mugglestone, M. A., & Meechan, D. F. (2003). Health effects of a sulphur dioxide air pollution episode. *Journal of Public Health Medicine*, *25*(4), 369–371. https://doi.org/10.1093/pubmed/fdg083

Collivignarelli, M. C., Abbà, A., Bertanza, G., Pedrazzani, R., Ricciardi, P., & Carnevale Miino, M. (2020). Lockdown for CoViD-2019 in Milan: What are the effects on air quality? *Science of the Total Environment*, *732*(February), 139280. https://doi.org/10.1016/j.scitotenv.2020.139280

Cui, J., Pandey Deolal, S., Sprenger, M., Henne, S., Staehelin, J., Steinbacher, M., & Nédélec, P. (2011). Free tropospheric ozone changes over Europe as observed at Jungfraujoch (1990-2008): An analysis based on backward trajectories. *Journal of Geophysical Research Atmospheres*, *116*(10), 1–14. https://doi.org/10.1029/2010JD015154

D.C.Catling. (2015). Planetary Atmospheres. In G. Schubert (Ed.), *Treatise on Geophysics* (Second Edi, pp. 429–472). Elsevier. https://doi.org/10.1016/B978-0-444-53802-4.00185-8.

Dickson, D., Hardin, K., & Mittal, A. (2020). *The great compression: Implications of COVID-19 for the US shale industry*.

Donnell, E. A., Fish, D. J., Dicks, E. M., & Thorpe, A. J. (2001). Mechanisms for pollutant transport between the boundary layer and the free troposphere. *Journal of Geophysical Research Atmospheres*, *106*(D8), 7847–7856. https://doi.org/10.1029/2000JD900730

European Environment Agency (EEA) 2020 Air pollutant emissions data viewer. (2020). Gothenburg Protocol, LRTAP Convention. https://doi.org/10.15196/TS600305

European Union Publications Office. (n.d.). *Directive 2004/42/CE of the European Parliament and the Council*. 2019 Update.

Evangeliou, N., Platt, S. M., Eckhardt, S., Lund Myhre, C., Laj, P., Alados-Arboledas, L., Backman, J., Brem, B. T., Fiebig, M., Flentje, H., Marinoni, A., Pandolfi, M., Yus-Dìez, J., Prats, N., Putaud, J. P., Sellegri, K., Sorribas, M., Eleftheriadis, K., Vratolis, S., … Stohl, A. (2021). Changes in black carbon emissions over Europe due to COVID-19 lockdowns. *Atmospheric Chemistry and Physics*, *21*(4), 2675–2692. https://doi.org/10.5194/acp-21-2675-2021

Franco, B., Mahieu, E., Emmons, L. K., Tzompa-Sosa, Z. A., Fischer, E. V., Sudo, K., Bovy,

B., Conway, S., Griffin, D., Hannigan, J. W., Strong, K., & Walker, K. A. (2016). Evaluating ethane and methane emissions associated with the development of oil and natural gas extraction in North America. *Environmental Research Letters*, *11*(4). https://doi.org/10.1088/1748-9326/11/4/044010

Franco, Bruno, A Marais, E., Bovy, B., Bader, W., Lejeune, B., Roland, G., Servais, C., & Mahieu, E. (2016). Diurnal cycle and multi-decadal trend of formaldehyde in the remote atmosphere near 46°N. *Atmospheric Chemistry and Physics*, *16*(6), 4171–4189. https://doi.org/10.5194/acp-16-4171-2016

Gardiner, T., Forbes, A., De Mazière, M., Vigouroux, C., Mahieu, E., Demoulin, P., Velazco, V., Notholt, J., Blumenstock, T., Hase, F., Kramer, I., Sussmann, R., Stremme, W., Mellqvist, J., Strandberg, A., Ellingsen, K., & Gauss, M. (2008). Trend analysis of greenhouse gases over Europe measured by a network of ground-based remote FTIR instruments. *Atmospheric Chemistry and Physics*, *8*(22), 6719–6727. https://doi.org/10.5194/acp-8-6719-2008

Gatz, D., & Smith, L. E. (1995). The standard error of a weighted mean concentration—II. Estimating confidence intervals. *Atmospheric Environment*, *29*, 1195–1200.

Goldberg, D. L., Anenberg, S. C., Griffin, D., McLinden, C. A., Lu, Z., & Streets, D. G. (2020). Disentangling the Impact of the COVID-19 Lockdowns on Urban NO2 From Natural Variability. *Geophysical Research Letters*, *47*(17). https://doi.org/10.1029/2020GL089269

Guevara, M., Jorba, O., Soret, A., Petetin, H., Bowdalo, D., Serradell, K., Tena, C., Van Der Gon, H. D., Kuenen, J., Peuch, V. H., & Pérez Garciá-Pando, C. (2021). Time-resolved emission reductions for atmospheric chemistry modelling in Europe during the COVID-19 lockdowns. *Atmospheric Chemistry and Physics*, *21*(2), 773–797. https://doi.org/10.5194/acp-21-773-2021

Haagen-Smit, A. J., & Fox, M. M. (1954). Photochemical ozone formation with hydrocarbons and automobile exhaust. *Air Repair*, *4*(3), 105–136. https://doi.org/10.1080/00966665.1954.10467649

Hari, V., Rakovec, O., Markonis, Y., Hanel, M., & Kumar, R. (2020). Increased future occurrences of the exceptional 2018–2019 Central European drought under global warming. *Scientific Reports*, *10*(1), 1–10. https://doi.org/10.1038/s41598-020-68872-9

Hase, F., Hannigan, J. W., Coffey, M. T., Goldman, A., Höpfner, M., Jones, N. B., Rinsland, C. P., & Wood, S. W. (2004). Intercomparison of retrieval codes used for the analysis of

high-resolution, ground-based FTIR measurements. *Journal of Quantitative Spectroscopy and Radiative Transfer*, *87*(1), 25–52. https://doi.org/10.1016/j.jqsrt.2003.12.008

Heald, C. L., & Kroll, J. H. (2020). The fuel of atmospheric chemistry: Toward a complete description of reactive organic carbon. *Science Advances*, *6*(6), 1–9. https://doi.org/10.1126/sciadv.aay8967

Heilig, G. K. (1994). The greenhouse gas methane (CH4): Sources and sinks, the impact of population growth, possible interventions. *Population and Environment*, *16*(2), 109–137. https://doi.org/10.1007/BF02208779

Helmig, D., Rossabi, S., Hueber, J., Tans, P., Montzka, S., Masarie, K., Thoning, K., Plass-Duelmer, C., Claude, A., Carpenter, L., Lewis, A., Punjabi, S., Reimann, S., Vollmer, M., Steinbrecher, R., Hannigan, J., Emmons, L., Mahieu, E., Franco, B., & Pozzer, A. (2016). Reversal of global atmospheric ethane and propane trends largely due to US oil and natural gas production. *Nature Geoscience*, *9*. https://doi.org/10.1038/NGEO2721

Hendrick, F., Mahieu, E., Bodeker, G. E., Boersma, K. F., Chipperfield, M. P., De Mazière, M., De Smedt, I., Demoulin, P., Fayt, C., Hermans, C., Kreher, K., Lejeune, B., Pinardi, G., Servais, C., Stübi, R., Van Der A, R., Vernier, J. P., & Van Roozendael, M. (2012). Analysis of stratospheric NO2 trends above Jungfraujoch using ground-based UV-visible, FTIR, and satellite nadir observations. *Atmospheric Chemistry and Physics*, *12*(18), 8851–8864. https://doi.org/10.5194/acp-12-8851-2012

Inglezakis, V. J., Poulopoulos, S. G., Arkhangelsky, E., Zorpas, A. A., & Menegaki, A. N. (2016). Aquatic Environment. In *Environment and Development*. Elsevier B.V. https://doi.org/10.1016/b978-0-444-62733-9.00003-4

International Organisation for Standardisation. (1975). *ISO 2533:1975 Standard Atmosphere*.

Kasuga, H. (1989). Health effects of air pollution Particulate Matter, Ozone and Nitrogen Dioxide. *How to Conquer Air Pollution: A Japanese Experience*, *January*, 95–113. https://doi.org/10.1016/s0140-6736(05)77146-4

Keller, M. D., Bellows, W. K., & Guillard, R. R. L. (1989). *Dimethyl Sulfide Production in Marine Phytoplankton*. *May*, 167–182. https://doi.org/10.1021/bk-1989-0393.ch011

Kerimray, A., Baimatova, N., Ibragimova, O. P., Bukenov, B., Kenessov, B., Plotitsyn, P., & Karaca, F. (2020). Assessing air quality changes in large cities during COVID-19 lockdowns: The impacts of traffic-free urban conditions in Almaty, Kazakhstan. *Science of the Total Environment*, *730*, 139179. https://doi.org/10.1016/j.scitotenv.2020.139179

Kirschke, S., Bousquet, P., Ciais, P., Saunois, M., Canadell, J. G., Dlugokencky, E. J., Bergamaschi, P., Bergmann, D., Blake, D. R., Bruhwiler, L., Cameron-Smith, P., Castaldi, S., Chevallier, F., Feng, L., Fraser, A., Heimann, M., Hodson, E. L., Houweling, S., Josse, B., … Zeng, G. (2013). Three decades of global methane sources and sinks. *Nature Geoscience*, *6*(10), 813–823. https://doi.org/10.1038/ngeo1955

Le Quéré, C., Jackson, R. B., Jones, M. W., Smith, A. J. P., Abernethy, S., Andrew, R. M., De-Gol, A. J., Willis, D. R., Shan, Y., Canadell, J. G., Friedlingstein, P., Creutzig, F., & Peters, G. P. (2020). Temporary reduction in daily global CO2 emissions during the COVID-19 forced confinement. *Nature Climate Change*, *10*(7), 647–653. https://doi.org/10.1038/s41558-020-0797-x

Lelieveld, J., Peters, W., Dentener, F. J., & Krol, M. C. (2002). Stability of tropospheric hydroxyl chemistry. *Journal of Geophysical Research: Atmospheres*, *107*(D23), 1–11. https://doi.org/10.1029/2002JD002272

Li, Q., Palmer, P. I., Pumphrey, H. C., Bernath, P., & Mahieu, E. (2009). What drives the observed variability of HCN in the troposphere and lower stratosphere? *Atmospheric Chemistry and Physics*, *9*(21), 8531–8543. https://doi.org/10.5194/acp-9-8531-2009

Liu, Z., Ciais, P., Deng, Z., Lei, R., Davis, S. J., Feng, S., Zheng, B., Cui, D., Dou, X., Zhu, B., Guo, R., Ke, P., Sun, T., Lu, C., He, P., Wang, Y., Yue, X., Wang, Y., Lei, Y., … Schellnhuber, H. J. (2020). Near-real-time monitoring of global CO2 emissions reveals the effects of the COVID-19 pandemic. *Nature Communications*, *11*(1), 1–12. https://doi.org/10.1038/s41467-020-18922-7

Mahato, S., Pal, S., & Ghosh, K. G. (2020). Effect of lockdown amid COVID-19 pandemic on air quality of the megacity Delhi, India. *Science of the Total Environment*, *730*, 139086. https://doi.org/10.1016/j.scitotenv.2020.139086

Mahieu, E., Franco, B., Pozzer, A., Taraborrelli, D., Bader, W., Prignon, M., & Servais, C. (2018). Observation and simulation of ethane at 23 FTIR sites. *Geophysical Research Abstracts*, *20*. https://doi.org/10.1073/pnas.1616020114

Migeotte, M. and L. N. (1950). Détection du monoxide de carbonne dans l'atmosphère terrestre à 3580 mètres d'altitude. In *Physica 16*.

Miller, B. (2015). Sulfur oxides formation and control. In *Fossil Fuel Emissions Control Technologies* (Issue base 10). https://doi.org/10.1016/b978-0-12-801566-7.00004-x

Montero-Montoya, R., López-Vargas, R., & Arellano-Aguilar, O. (2018). Volatile organic compounds in air: Sources, distribution, exposure and associated illnesses in children.

Annals of Global Health, *84*(2), 225–238. https://doi.org/10.29024/aogh.910

Murray, L. T. (2016). Lightning NOx and Impacts on Air Quality. *Current Pollution Reports*, *2*(2), 115–133. https://doi.org/10.1007/s40726-016-0031-7

National Research Council. (1991). VOCs and NOx: Relationship to Ozone and Associated Pollutants. In *Rethinking the Ozone Problem in Urban and Regional Air Pollution.* (pp. 163–168).

Nielsen, A. H. and M. M. (1952). Abundance and verticale distribution of tellutic methane from measurements at 3580 meters elevation. *Ann. Astrophys*, *15*, 134–141.

NOAA National Centers for Environmental information. (2021). *Climate at a Glance: Global Time Series*. https://www.ncdc.noaa.gov/cag/

Ordóñez, C., Garrido-Perez, J. M., & García-Herrera, R. (2020). Early spring near-surface ozone in Europe during the COVID-19 shutdown: Meteorological effects outweigh emission changes. *Science of the Total Environment*, *747*(December 2019), 141322. https://doi.org/10.1016/j.scitotenv.2020.141322

Peters, G. P., Andrew, R. M., Canadell, J. G., Friedlingstein, P., Jackson, R. B., Korsbakken, J. I., Le Quéré, C., & Peregon, A. (2020). Carbon dioxide emissions continue to grow amidst slowly emerging climate policies. *Nature Climate Change*, *10*(1), 3–6. https://doi.org/10.1038/s41558-019-0659-6

Rinsland, C. P., Jones, N. B., Connor, B. J., Logan, J. a, Pougatchev, N. S., Goldman, A., Murcray, F. J., Stephen, T. M., Pine, A. S., Zander, R., Mahieu, E., & Demoulin, P. (1998). *Spectroscopic Measurements of Tropospheric Seasonal Variations Inithe Lower Layer With Trends Equal*. *103*(November 1981).

Rose, J. J., Wang, L., Xu, Q., McTiernan, C. F., Shiva, S., Tejero, J., & Gladwin, M. T. (2017). Carbon monoxide poisoning: Pathogenesis, management, and future directions of therapy. *American Journal of Respiratory and Critical Care Medicine*, *195*(5), 596–606. https://doi.org/10.1164/rccm.201606-1275CI

Royal Belgian Institute for Space Aeronomy. (n.d.). *Troposphere, main gases, composition and abundance*. Retrieved April 22, 2021, from https://www.aeronomie.be/en/encyclopedia/troposphere-main-gases-composition-and-abundance

Sannigrahi, S., Kumar, P., Molter, A., Zhang, Q., Basu, B., Basu, A. S., & Pilla, F. (2021). Examining the status of improved air quality in world cities due to COVID-19 led temporary reduction in anthropogenic emissions. *Environmental Research*,

196(September 2020), 110927. https://doi.org/10.1016/j.envres.2021.110927

Schaefer, H. (2019). On the Causes and Consequences of Recent Trends in Atmospheric Methane. *Current Climate Change Reports*, *5*(4), 259–274. https://doi.org/10.1007/s40641-019-00140-z

Schumann, U., & Huntrieser, H. (2007). The global lightning-induced nitrogen oxides source. *Atmospheric Chemistry and Physics*, *7*(14), 3823–3907. https://doi.org/10.5194/acp-7-3823-2007

Shuai, J., Kim, S., Ryu, H., Park, J., Lee, C. K., Kim, G. B., Ultra, V. U., & Yang, W. (2018). Health risk assessment of volatile organic compounds exposure near Daegu dyeing industrial complex in South Korea. *BMC Public Health*, *18*(1), 1–13. https://doi.org/10.1186/s12889-018-5454-1

Siciliano, B., Dantas, G., da Silva, C. M., & Arbilla, G. (2020). Increased ozone levels during the COVID-19 lockdown: Analysis for the city of Rio de Janeiro, Brazil. *Science of the Total Environment*, *737*, 139765. https://doi.org/10.1016/j.scitotenv.2020.139765

Simpson, I. J., Andersen, M. P. S., Meinardi, S., Bruhwiler, L., Blake, N. J., Helmig, D., Sherwood Rowland, F., & Blake, D. R. (2012). Long-term decline of global atmospheric ethane concentrations and implications for methane. *Nature*, *488*(7412), 490–494. https://doi.org/10.1038/nature11342

Smith, F. B. (1975). Turbulence in the atmospheric boundary layer. *Science Progress (1933-)*, *62*(245), 127–151. http://www.jstor.org/stable/43420288

Steinbrecht, W., Kubistin, D., Plass-Dülmer, C., Davies, J., Tarasick, D. W., Gathen, P. von der, Deckelmann, H., Jepsen, N., Kivi, R., Lyall, N., Palm, M., Notholt, J., Kois, B., Oelsner, P., Allaart, M., Piters, A., Gill, M., Van Malderen, R., Delcloo, A. W., … Cooper, O. R. (2021). COVID-19 Crisis Reduces Free Tropospheric Ozone Across the Northern Hemisphere. *Geophysical Research Letters*, *48*(5). https://doi.org/10.1029/2020GL091987

Stull, R. B. (1988). *An introduction to boundary layer meteorology* (Volume 1).

Sun, W., Zhu, L., De Smedt, I., Bai, B., Pu, D., Chen, Y., Shu, L., Wang, D., Fu, T. M., Wang, X., & Yang, X. (2021). Global Significant Changes in Formaldehyde (HCHO) Columns Observed From Space at the Early Stage of the COVID-19 Pandemic. *Geophysical Research Letters*, *48*(4). https://doi.org/10.1029/2020GL091265

Van Damme, M., Clarisse, L., Franco, B., Sutton, M. A., Erisman, J. W., Wichink Kruit, R., van Zanten, M., Whitburn, S., Hadji-Lazaro, J., Hurtmans, D., Clerbaux, C., & Coheur,

P.-F. (2020). Global, regional and national trends of atmospheric ammonia derived from a decadal (2008-2018) satellite record. *Environmental Research Letters*. https://doi.org/10.1088/1748-9326/abd5e0

van Zanten, M. C., Wichink Kruit, R. J., Hoogerbrugge, R., Van der Swaluw, E., & van Pul, W. A. J. (2017). Trends in ammonia measurements in the Netherlands over the period 1993–2014. *Atmospheric Environment*, *148*, 352–360. https://doi.org/10.1016/j.atmosenv.2016.11.007

Venter, Z. S., Aunan, K., Chowdhury, S., & Lelieveld, J. (2020). COVID-19 lockdowns cause global air pollution declines with implications for public health risk. *MedRxiv*, *7162*. https://doi.org/10.1101/2020.04.10.20060673

Vigouroux, C., Blumenstock, T., Coffey, M., Errera, Q., Garciá, O., Jones, N. B., Hannigan, J. W., Hase, F., Liley, B., Mahieu, E., Mellqvist, J., Notholt, J., Palm, M., Persson, G., Schneider, M., Servais, C., Smale, D., Thölix, L., & De Mazière, M. (2015). Trends of ozone total columns and vertical distribution from FTIR observations at eight NDACC stations around the globe. *Atmospheric Chemistry and Physics*, *15*(6), 2915–2933. https://doi.org/10.5194/acp-15-2915-2015

Weber, J., Shin, Y. M., Staunton Sykes, J., Archer-Nicholls, S., Abraham, N. L., & Archibald, A. T. (2020). Minimal Climate Impacts From Short-Lived Climate Forcers Following Emission Reductions Related to the COVID-19 Pandemic. *Geophysical Research Letters*, *47*(20). https://doi.org/10.1029/2020GL090326

World Health Organization. (1980). Glossary on air pollution. In *Glossary on air pollution.* (Issue 9). https://doi.org/10.1016/0160-4120(81)90119-7

World Meteorological Organization (WMO). (2020). *Arctic ozone depletion reached record level*. WMO Website. https://public.wmo.int/en/media/news/arctic-ozone-depletion-reached-record-level

Wu, X. (May), Fana, Z. (Tina), Zhua, X., Junga, K. H., Pamela Ohman-Stricklanda, C. P. W., & Lioy, P. J. (2012). Exposures to volatile organic compounds (VOCs) and associated health risks of socio-economically disadvantaged population in a “hot spot” in Camden, New Jersey. *Atmos Environ*, *57*, 72–79. https://doi.org/10.1016/j.atmosenv.2012.04.029.Exposures

Xiao, Y., Logan, J. A., Jacob, D. J., Hudman, R. C., Yantosca, R., & Blake, D. R. (2008). Global budget of ethane and regional constraints on U.S. sources. *Journal of Geophysical Research Atmospheres*, *113*(21), 1–13.

https://doi.org/10.1029/2007JD009415

Yao, X., & Zhang, L. (2019). Causes of Large Increases in Atmospheric Ammonia in the Last Decade across North America. *ACS Omega*, *4*(26), 22133–22142. https://doi.org/10.1021/acsomega.9b03284

Yokelson, R. J. (1999). Emissions of formaldehyde, acetic acid, methanol, and other trace gases from biomass fires in North Carolina measured by airborne Fourier transform infrared spectroscopy. *Journal of Geophysical Research Atmospheres*, *104*(D23), 30109–30125. https://doi.org/10.1029/1999JD900817

Zhu, L., Henze, D. K., Bash, J. O., Cady-Pereira, K. E., Shephard, M. W., Luo, M., & Capps, S. L. (2015). Sources and Impacts of Atmospheric NH3: Current Understanding and Frontiers for Modeling, Measurements, and Remote Sensing in North America. *Current Pollution Reports*, *1*(2), 95–116. https://doi.org/10.1007/s40726-015-0010-4

Zong, R., Yang, X., Wen, L., Xu, C., Zhu, Y., Chen, T., Yao, L., Wang, L., Zhang, J., Yang, L., Wang, X., Shao, M., Zhu, T., Xue, L., & Wang, W. (2018). Strong ozone production at a rural site in theNorth China Plain: Mixed effects of urban plumesand biogenic emissions. *Journal of Environmental Sciences (China)*, *71*, 261–270. https://doi.org/10.1016/j.jes.2018.05.003